Index

North Sea FLOW Measurement Workshop

Paper 6.1

Pressure and Temperature Effects for Ormen Lange Ultrasonic Gas Flow Meters – Results from a Follow-Up Study

Per Lunde
University of Bergen

Kjell-Eivind Frøysa
Christian Michelsen Research AS (CMR)

Vincent Martinez and Øyvind Torvanger
CMR Prototech

TÜV SÜD

nel technology for life

Pressure and Temperature Effects for Ormen Lange Ultrasonic Gas Flow Meters - Results from a Follow-up Study

Per Lunde, University of Bergen
Kjell-Eivind Frøysa, Christian Michelsen Research AS (CMR)
Vincent Martinez, CMR Prototech
Øyvind Torvanger, CMR Prototech

ABSTRACT

Ultrasonic gas flow meters may be influenced by pressure and temperature in several ways. Change of the meter body's cross-sectional area (the "pipe bore") influences directly on the amount of gas flowing through the meter. Change of the ultrasonic path geometry (i.e. change of the inclination angles and lateral chord positions, caused by e.g. spoolpiece diameter change and change of the orientation of the ultrasonic transducer ports) influences on the transit times and the numerical integration method of the meter. Change of the Reynolds number influences on the integration method. Change of the length of the ultrasonic transducer ports influences on the acoustic path lengths, and thus on the transit times. Likewise, change of the length of the ultrasonic transducers influences on the acoustic path lengths, and thus on the transit times. In addition, changes of the transducer properties such as the directivity, influences on the diffraction correction, and thus on the transit times.

Some of these issues are addressed to some extent in current draft standards for such meters, such as the AGA-9 (1998) report, and the ISO/CD 17089-1 (2007). Other of these effects have not been described or treated in the literature.

In 2007, a paper was given at the NSFMW'07 [2] on pressure and temperature effects for five 18" Instromet Q-Sonic 5 ultrasonic flow meters (USMs) operated in the Ormen Lange fiscal metering system at Nyhamna in Møre and Romsdal, Norway, from October 2007. Pressure and temperature changes from flow calibration (Westerbork, at 63 barg and 7 ^{o}C) to field operation (Ormen Lange, nominally at 230 barg and 40 ^{o}C) conditions were evaluated. The effects addressed were changes related to (A) the meter's cross-sectional area, (B) the ultrasonic path geometry (inclination angles and lateral chord positions), (C) length expansion of the ultrasonic transducer ports, (D) length expansion/compression of the ultrasonic transducers, and (E) Reynolds number correction.

The various effects (A)-(E) contributing to the measurement error were discussed and quantified. Investigations were made using a combination of analytical modeling and finite element numerical modeling (FEM) of the meter body and the ultrasonic transducers, combined with a model for USM numerical integration relevant for the Q-Sonic 5 multipath ultrasonic flow meter in question.

Two correction factors were proposed for the Q-Sonic 5 in this application: (1) one "nominal P&T correction factor" (accounting for by far the largest part of the correction, about 0.26 %), and (2) an "instantaneous P&T correction factor" (accounting for small deviations in pressure and temperature from nominal to actual Ormen Lange conditions), which is typically an order of magnitude smaller than the nominal P&T correction factor. The correction factors and the individual contributors to these were discussed and quantified.

There has been raised some questions (cf. e.g. [3]) in relation to the results presented in [1,2], and on basis of such discussions, a follow-up study has been initiated.

In the present paper, pressure effects on the meter body related to the effects (A) and (B) have been revisited and analysed in more detail, for three different "meter body geometries", cylindrical pipe, flanged pipe, and flanged pipe with ultrasonic transducer ports (the Ormen Lange Q-Sonic 5 meter body). These cases have been analyzed with respect to influence of axial boundary conditions ("ends free", "ends clamped", "ends capped"), and influence of the

meter body wall thicknesses. A combination of finite element modelling (FEM) and analytical modelling has been used for this purpose.

It has been found that with respect to pressure effects on the inner radius displacement, the cylindrical pipe thick-shell model (cf. "Roark formuls") with either "ends free" or "ends capped" axial boundary conditions provides a good approximation for all three "meter body geometries" considered here, for wall thicknesses up to $w/R_0 = 0.25$. The corresponding thin-shell models (cf. "Roark formulas") represent relatively poor approximations in the range $w/R_0 = 0.05 - 0.25$.

The results show that for the Ormen Lange project, the actual axial boundary condition being used ("ends free", "ends clamped" or "ends capped") is not critical for calculation of the radial displacement and the pressure correction factor. That is, the boundary conditions approach taken in [1,2], where the "ends free" boundary condition was used, should be a valid and relatively accurate approach. For the Ormen Lange meter, the uncertainty of the volumetric flow rate measurement due to the choice of axial boundary condition made in the calculation of the "nominal P&T correction factor", is estimated to about ±0.01 %.

1 INTRODUCTION

From October 2007 five 18" Elster-Instromet Q-Sonic ultrasonic gas flow meters (USMs) have been operated at a land based fiscal gas metering station at Nyhamna, Møre and Romsdal, Norway, for export of gas through the 1200 km Langeled pipeline, to an import metering station in Easington, UK, built by Statoil, cf. Fig.1. The Ormen Lange export station at Nyhamna was constructed and built by Norsk Hydro, and is now operated by Shell. The production life of Ormen Lange is estimated to 50 years.

The nominal flow rate of the Ormen Lange export metering station is 70 million Sm^3/day, or 25 billion Sm^3/year. At an assumed sales price of 2 NOK/Sm^3 this corresponds tentatively to 140 million NOK/day, or 50 billion NOK/year. An assumed systematic measurement error of only 0.3 % (as an example), would correspond to about 420 000 NOK/day, or about 153 million NOK/year, for such a tentative sales price.

Flow calibration of the flow meters have been made at the Westerbork laboratory in the Netherlands, at temperature and pressure conditions of 7 ^oC og 63 barg, respectively, with two meters in series installed in a "long pipe", and with flow conditioner upstream of the meters.

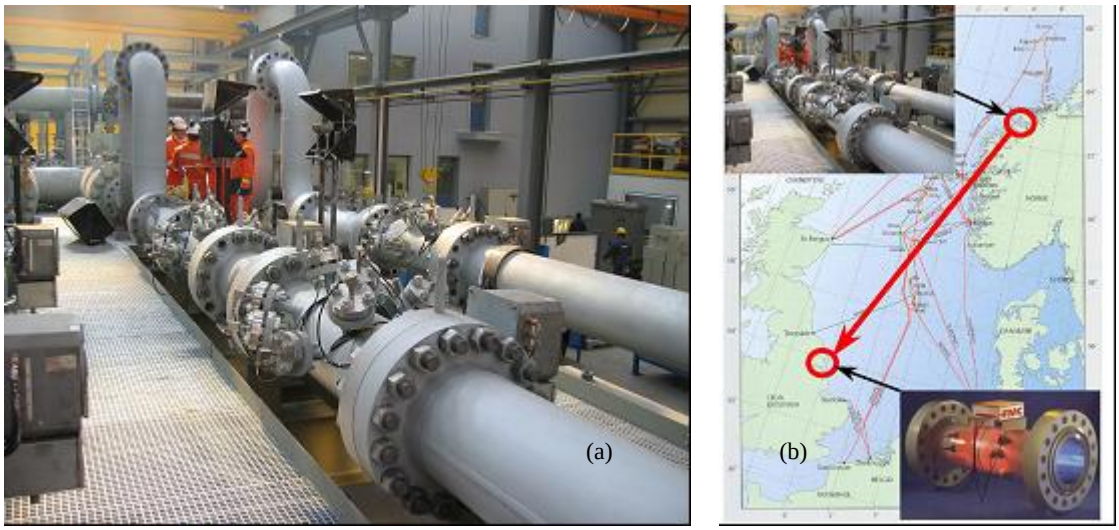

Fig. 1. (a) Photograph of the Ormen Lange fiscal gas metering station, under factory acceptance test (FAT) in Athens, Greece, 2005. (After [1,2].)
(b) Sketch of the Ormen Lange transport system, with fiscal metering stations at Nyhamna (Norway) and Easington (UK). (After [1,2].)

The high pressures in question at the Ormen Lange metering station, 230 barg nominal, have raised the question whether correction for pressure and temperature effects on the USMs will be needed, relative to the 63 barg pressure used under flow calibration at Westerbork.

Pressure and temperature effects on the ultrasonic meters relates to factors such as e.g.

(A) Change of the meter's cross-sectional area,
(B) Change of the ultrasonic path geometry (inclination angles and lateral chord positions),
(C) Change of the length of the ultrasonic transducer ports,
(D) Change of the length of the ultrasonic transducers,
(E) Change of the Reynolds number,
(F) Diffraction correction effects.

In [1,2], the various effects (A)-(E) contributing to the measurement error have been analyzed and quantified. Investigations were made using a combination of analytical modeling and finite element numerical modeling of the meter body and the ultrasonic transducers, combined with a model for USM numerical integration relevant for the Q-Sonic 5 multipath ultrasonic flow meter in question.

In [1,2], two correction factors were proposed for the Q-Sonic 5 in this application:

(1) a "nominal P&T correction factor" (accounting for by far the largest part of the correction, about 0.26 %), and
(2) an "instantaneous P&T correction factor" (accounting for small deviations in pressure and temperature from nominal to actual Ormen Lange conditions), which is typically an order of magnitude smaller than the nominal P&T correction factor.

The correction factors and the individual contributors to these were discussed and quantified. It was concluded that for the Ormen Lange application, evaluation of all of the factors (A)-(E) are necessary to establish the effect of pressure and temperature on the meter. Finite element modeling (FEM) calculations indicated that the combined effect of (A) change of the meter's cross-sectional area (diameter change) and (B) change of the ultrasonic path geometry (inclination angles and lateral chord positions) are by far the largest and most dominant effects, amounting to about 0.246 %. Of this number, the pressure and temperature effects were found to be responsible for 0.121 % and 0.125 %, respectively. The total effect of (A) – (E) was calculated to be 0.262 % (the "nominal P&T correction factor").

There has been raised some questions (cf. e.g. [3]) in relation to the results presented in [1,2], and on basis of such discussions, a follow-up (Phase 2) study has been initiated by Shell on behalf of the Ormen Lange partners, on an initiative from the Norwegian Petroleum Directorate (NPD). The follow up-study is carried out by Christian Michelsen Research AS (CMR) in cooperation with the University of Bergen, Norway.

In the present paper, selected and central topics from this follow-up study are addressed. The analysis and discussion is here limited to the effects (A) and (B) in the list above, since these are by far the dominating sources of measurement error in the Ormen Lange application [1,2]. Moreover, the present analysis is limited to pressure effects, since there has been no remarks in relation to the way temperature effects are treated in [1,2]. The temperature correction was made in agreement with ISO/CD 17089-1 recommendations [6].

The topics addressed here in relation to pressure effects on (A) and (B) are:

- For the FEM analysis on which the "nominal P&T correction factor" was based in [1,2], "ends free" boundary conditions were used at the meter body ends. Boundary conditions play a major role in the outcome of any FEM exercise, and - since the approach used in [1,2] may be questioned [3] - a number of scenarios are run here to investigate the sensitivity of the results to different boundary conditions. Four different axial boundary conditions are investigated: (a) "ends free", (b) "ends clamped", (c) "ends capped (bolt circle curve load)" and (d) "ends capped (flange surface load)" (cf. Section 3.1).

- For the comparably small and significantly less important "instantaneous P&T correction factor", a thin-wall pipe theory was used in [1,2]. Thus, this thin-wall theory was used only for very small pressure changes (a few bars). However, it has been commented [3] that since the actual meter body is clearly a thick-wall vessel (the thickness/radius ratio of the body is 0.25 while the indicated "thin-wall limit" is 0.1 [5]), the estimation of the deflection using thin-wall theory may be questioned. Comparison of thin- and thick-wall theories with FEM results are thus made here, to investigate the need for using thick-wall theory for the relatively small pressure effects in the "instantaneous P&T correction factor".

The objective of the present paper is thus - through a more refined and extended FEM analysis of pressure effects on the meter body - to get improved insight into the validity and accuracy of the analysis and results presented in [1,2].

2 SPECIFICATIONS

The specifications for the study are the same as in [1,2], repeated here for convenience and completeness.

The Ormen Lange metering station consists of 3 parallel meter runs, with in total 5 ultrasonic flow meters, cf. Fig. 1:

- 2 parallel runs, each with two 18" ultrasonic flow meters in series,
- 1 parallel run with one 18" ultrasonic flow meter, for backup measurement,
- Flow conditioner will be used (DN450 Laws type 316SS or Duplex Material),
- Elster-Instromet Q-Sonic 5 ultrasonic gas flow meters [4].

Table 1 gives various parameters of the USM, and Table 2 other specifications for the study. For other details on the Q-Sonic 5 meter of relevance for the study, it is referred to [1,2].

With respect to the topic under study here, it is noted that the pressure change from Westerbork (flow calibration) to nominal Ormen Lange (operating) conditions is ΔP_{mc} = (230 – 63) bar = 167 bar, cf. Table 2.

Table 1. Specifications of the ultrasonic flow meters used in the Ormen Lange metering station.

Parameter	Property	Conditions
Material type	Steel (Duplex)	
Length, L_0	1800 mm	(at assumed 20 °C, 1 atm.)
Outer diameter, *OD*	457.2 mm	(at assumed 20 °C, 1 atm.)
Inner diameter, *ID*	(366.5 ± 0.25) mm	(at assumed 20 °C, 1 atm.)
Inner radius, R_0	183.25 mm	(at assumed 20 °C, 1 atm.)
Wall thickness, *w*	45.35 mm	(at assumed 20 °C, 1 atm.)
w/R_0	0.25	(at assumed 20 °C, 1 atm.)
Young's modulus, *Y*	$2.0 \cdot 10^5$ MPa	
Poisson's ratio, σ	0.3	
Coeff. of linear thermal expansion, α	$12.6 \cdot 10^{-6}$ K^{-1} (ASME)	

Table 2. Specifications for the study.

Parameter	Westerbork flow calibration conditions	Ormen Lange metering station (line conditions, nominal)
Gas	Dry natural gas	Dried natural gas[a)]
Pressurel *P*	63 barg	230 barg (design)
Temperature	7 °C	40 °C (design)
Viscosity	$1.30 \cdot 10^{-5}$ Pa-s	$2.28 \cdot 10^{-5}$ Pa-s
Density	57.36 kg/m^3	186.6 kg/m^3
Metering configuration	2 USMs in series, with upstream flow conditioner	2 USMs in series, with upstream flow conditioner
Flow velocity	1.5 – 19 m/s	Volumetric flow rate 70 MSm^3/d (=> flow velocity = 15-16 m/s per run)
Reynolds number, *Re*	$2.4 \cdot 10^6$ – $3.0 \cdot 10^7$	$4.5 \cdot 10^7$

[a)] The gas composition is known, but has not been necessary to specify for the present study.

3 ANALYSIS METHODS

The analysis methods used in the study are described in the following.

3.1 Boundary Conditions (Axial Constraints)

The deformations of the meter body are quite dependent on how the pipe is constrained. To investigate the sensitivity of the results to different boundary conditions, three different cases of axial constraint are studied: (a) "ends free", (b) "ends clamped", and (c) "ends capped".

”Ends free” boundary conditions imply that the spool is free to deform axially, and that the interior pressure does not induce any axial loads. An example of this case is a pressurized pipe where at least one of the ends is resting on an o-ring or another dynamic seal. In a straight pipe the pressure will only cause tangential tensile stresses. The pipe will contract in the axial direction due to the Poisson effect.

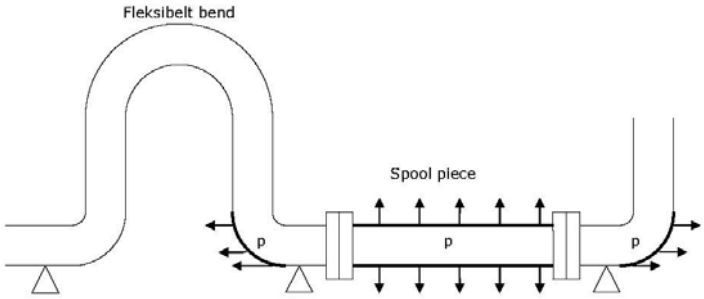

Fig. 2. Sketch of pipeline section in which the meter is mounted, illustrating the loads on a meter body (spoolpiece) due to pressure. The pipe is free to slide on the supports.

”Ends clamped” boundary conditions imply that the spool is fixed against axial movement (no axial displacement at the two end surfaces of the pipe). An example of this case is a long straight rock dumped pipe. This pipe is not able to deform axially. The pressure will cause tangential tensile stresses, but also axial tensile stresses due to the Poisson effect. If this pipe is heated, the thermal expansion may cause axial compressive stresses, causing buckling if the rock dump is insufficient.

”Ends capped” boundary conditions imply that the spool is free to deform axially, and that the pressure also induces axial loads. An example of this case is a capped (closed) pipe (a pressure tank). An other example of this case is a pipe resting on sliding supports, connected to a flexible bend (cf. Fig. 2). The pressure will cause both tangential tensile stresses and axial tensile stresses. The axial stresses are caused by a pressure against an end cap or a bend, and are transferred through the bolts of the flanges. This is a common design of piping to avoid compressive stresses in the piping and to avoid large loads in the foundations. However, even in a flexible bend there will be some stiffness, causing axial stresses in the spool.

3.2 Simulation series overview

Table 3 gives an overview of the simulation series described in the present paper. Three different "meter body geometries" are considered: (a) a cylindrical (straight) pipe, (b) a flanged pipe, and (c) a flanged pipe with transducer ports (equal to the Ormen Lange Q-Sonic 5 meter body). All have the same length L_0 and inner radius R_0 at "dry calibration" conditions (20 ^{o}C, 1 atm., cf. Table 2), and the wall thickness / inner radius ratio w/R_0 is varied in five steps from 0.05 to 0.25, where the latter value relates to the Ormen Lange case.

In this study, each of these "meter body geometries" are subjected to different axial constraints, as described in Section 3.1: (a) "ends free", (b) "ends capped", and (c) "ends clamped". For all of these cases, finite element calculations (FEM) are made (cf. Section 3.4). In addition, analytical (simplified) theory is used whenever available (cf. Section 3.3).

Table 3. Meter body geometries, axial boundary conditions, and calculation analysis methods used in the present study.

Meter body geometry	Axial boundary conditions	Type of analysis
Cylindrical pipe	Ends free	• Thin shell theory (Roark) • Thick shell theory (Roark) • FEM
	Ends capped (tank)	• Thin shell theory (Roark) • Thick shell theory (Roark) • FEM
	Ends clamped	• FEM
Flanged pipe	Ends free	• FEM
	Ends capped (tank)	• FEM
	Ends clamped	• FEM
Flanged pipe, w/ transducer ports	Ends free	• FEM
	Ends capped (tank)	• FEM
	Ends clamped	• FEM
"Flanged-in meter body" (ISO 17089-1, 2007)	-	• Thin shell theory
"Welded-in meter body" (ISO 17089-1, 2007)	-	• Thin shell theory

3.3 Analytical calculation models

In ultrasonic transit time flow meters with reflecting and/or non-reflecting paths, the volumetric flow rate (at line conditions) is given as [6-8][1]

$$q_{USM} = \pi R^2 \sum_{i=1}^{N} w_i (N_{refl,i} + 1) \frac{2\sqrt{R^2 - y_i^2}\,(t_{1i} - t_{2i})}{t_{1i} t_{2i} \left|\sin 2\phi_i\right|} \,. \tag{1}$$

"Analytical model A". At a temperature T_m and pressure P_m, the meter body radius (R), the lateral chord positions (y_i), and the inclination angles (ϕ_i), can be shown to be approximately given by [8,1,2]

$$R \approx K_T K_P R_c \,, \qquad y_i \approx K_T K_P y_{ic} \,, \qquad \phi_i \approx \tan^{-1}\left(\frac{\tan(\phi_{ic})}{1 - (1 - \beta^* / \beta)(K_P - 1)} \right), \qquad i = 1, \ldots, N \tag{2}$$

where subscript "*c*" is used to denote the respective geometrical quantity at flow calibration (Westerbork) conditions, i.e. R_c, y_{ic} and ϕ_{ic}. The correction factors for the inner radius of the meter body due to dimensional changes caused by temperature and pressure changes relative to flow calibration conditions, are given as (cf. e.g. [9-12])

$$K_T \equiv 1 + \alpha \Delta T_{mc} \,, \qquad \Delta T_{mc} \equiv T_m - T_c \,, \tag{3}$$

$$K_P \equiv 1 + \beta \Delta P_{mc} \,, \qquad \Delta P_{mc} \equiv P_m - P_c \,, \tag{4}$$

respectively. Eqs. (2)-(4) are referred to as the "analytical model A" [1,2], and applies to all inclination angles.

[1] Symbols are defined at the end of the paper.

"Analytical model B". For USMs where all inclination angles are equal to ±45°, q_{USM} can - from Eqs. (1)-(4) - be written as [8,1]

$$q_{USM} \approx q_{USM,c} \cdot C_{tsm} \cdot C_{psm} \quad , \tag{5}$$

where

$$C_{tsm} = K_T^3 = (1+\alpha\Delta T_{mc})^3 \approx 1+3\alpha\Delta T_{mc}\,, \quad C_{psm} = K_P^3 = (1+\beta\Delta P_{mc})^3 \approx 1+3\beta\Delta P_{mc}\,. \tag{6}$$

Eqs. (5)-(6) are referred to as the "analytical model B" [1,2]. The main advantage of the analytical model B over model A lays in the fact that in model B, the *P* and *T* corrections of the geometrical quantities of the meter body can be separated from the basic USM functional relationship and put outside of the summing over paths, as illustrated by Eq. (5). For USMs with inclination angles equal to ±45°, the analytical model B is equivalent to the analytical model A. For other inclination angles it represents an approximation to the more accurate analytical model A [8]. This is the case for Q-Sonic 5, which employ inclination angles of 60° and 70°.

Table 4. Thin and thick cylindrical shell models, for different axial boundary conditions, taken from ref. [5] (Roark formulas), Table 13.1 (p. 592, cases 1b and 1c) and Table 13.5 (p. 683, cases 1a and 1b). (Blank fields: analytical theory not identified.)

Axial boundary conditions	Type of theory	$\frac{\Delta R}{R_0}$	$\frac{\Delta L}{L_0}$	β	β^*
Ends free	Thin shell	$\frac{\Delta R}{R_0} = \frac{R_0}{wY}\Delta P$	$\frac{\Delta L}{L_0} = -\frac{R_0\sigma}{wY}\Delta P$	$\beta = \frac{R_0}{wY}$	$\beta^* = -\frac{R_0\sigma}{wY}$
	Thick shell	$\frac{\Delta R}{R_0} = \frac{1}{Y}\left(\frac{(R_0+w)^2+R_0^2}{(R_0+w)^2-R_0^2}+\sigma\right)\Delta P$	$\frac{\Delta L}{L_0} = -\frac{\sigma}{Y}\frac{2R_0^2}{(R_0+w)^2-R_0^2}\Delta P$	$\beta = \frac{1}{Y}\left(\frac{(R_0+w)^2+R_0^2}{(R_0+w)^2-R_0^2}+\sigma\right)$	$\beta^* = -\frac{\sigma}{Y}\frac{2R_0^2}{(R_0+w)^2-R_0^2}$
Ends clamped	Thin shell		0		0
	Thick shell		0		0
Ends capped	Thin shell	$\frac{\Delta R}{R_0} = \frac{R_0}{wY}\left(1-\frac{\sigma}{2}\right)\Delta P$	$\frac{\Delta L}{L_0} = \frac{R_0}{wY}(0.5-\sigma)\Delta P$	$\beta = \frac{R_0}{wY}\left(1-\frac{\sigma}{2}\right)$	$\beta^* = \frac{R_0}{wY}(0.5-\sigma)$
	Thick shell	$\frac{\Delta R}{R_0} = \frac{1}{Y}\left(\frac{(R_0+w)^2(1+\sigma)+R_0^2(1-2\sigma)}{(R_0+w)^2-R_0^2}\right)\Delta P$	$\frac{\Delta L}{L_0} = \frac{1}{Y}\frac{R_0^2(1-2\sigma)}{(R_0+w)^2-R_0^2}\Delta P$	$\beta = \frac{1}{Y}\left(\frac{(R_0+w)^2(1+\sigma)+R_0^2(1-2\sigma)}{(R_0+w)^2-R_0^2}\right)$	$\beta^* = \frac{1}{Y}\frac{R_0^2(1-2\sigma)}{(R_0+w)^2-R_0^2}$

Coefficients of linear pressure expansion. The radial and axial linear pressure expansion coefficients β and β^* involved in the analytical models A and B depend on the type of support provided for the meter body installation (i.e. the boundary conditions). For cylindrical and isotropic elastic meter bodys, analytical models for β and β^* taken from the "Roark formulas" [5] are given in Table 4. For reference and to enable comparison, the two analytical models used in ISO/CD 17089-1 [6] are also included here, cf. Table 5.

Table 5. Thin shell models, for different pipe geometry / mounting conditions, taken from ref. [6] (ISO/CD 17089-1). (Blank fields: analytical theory not available.)

Mounting conditions	Type of theory	$\frac{\Delta R}{R_0}$	$\frac{\Delta L}{L_0}$	β	β^*
Flanged-in meter body	Thin shell	$\frac{\Delta R}{R_0} = 0.5\frac{R_0}{wY}\Delta P$		$\beta = 0.5\frac{R_0}{wY}$	
Welded-in meter body	Thin shell	$\frac{\Delta R}{R_0} = 1.17\frac{R_0}{wY}\Delta P$		$\beta = 1.17\frac{R_0}{wY}$	

3.4 Finite element modelling (FEM)

The analytical models A and B described in Section 3.3 represent simplified descriptions, accounting for "average" effects, and may in general not be able to account very precisely for the effects of pressure on the meter body. To analyze such effects in more detail and more accurately (including effects of flange thickness, wall thickness, the resulting form of the meter body (e.g. pipe bulging), influence of the transducer ports and their location, displacement of the transducer ports, precise calculation of the ultrasonic path lengths, etc.), a numerical finite element model (FEM) is needed.

Thus, as a second and considerably more accurate step to analyze pressure effects on the Q-Sonic 5 ultrasonic meter body, a FEM approach has been used. The finite element meshes used for FEM calculations of the three "meter body geometries" considered here are shown in Fig. 3. Dimensional changes caused by pressure changes, at any position of the meter body, may be calculated using FEM.

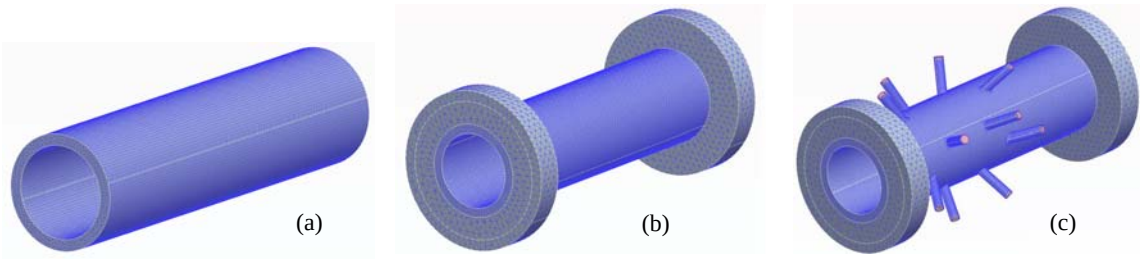

Fig. 3. Finite element mesh used for FEM analysis of P effects for (a) a cylindrical pipe, (b) a flanged pipe, and (c) flanged pipe with transducer ports (the Ormen Lange Q-Sonic 5 meter body).

For the calculations shown here, the NASTRAN (Version 2007.0.0 Release 1) finite element program is used, with the tetrahedral solid element CTETRA [7]. The end of the transducer ports are modelled using the shell elements CQUAD4 and CTRIA3, to enable extraction of the rotations at the transducer port extremities. The material data used for the calculations are given in Table 1.

The mesh control features used are the following:

- Maximum allowed element size: 40 mm for the flanges, 14 mm for the pipe, 4 mm for the transducer ports,
- Minimum forced element size: 20 mm for the flanges, 10 mm for the pipe, 2 mm for the transducer ports,
- Hard points with defined node identification (transducer port ends, and axial profile lines).

Three load cases are used, “ends free”, “ends clamped” and “ends capped”, cf. Section 3.1.

For the two cases “ends free” and “ends capped” the model is constrained against rigid body motion in all 6 degrees of freedom. The model is held in space, but it is free to deform under stress.

For the “ends clamped” case the model is also constrained against rigid body motion in all 6 degrees of freedom, but the flange end surfaces are additionally fully constrained against axial deformation. For the “ends capped” case, two different methods of applying the axial load are used: “bolt circle curve load” and “flange surface load”.

For the flanged pipe, an additional sub-load case is defined under the “ends free” and “ends capped” constraints, where the flanges are constrained against orthoaxial rotation. Rigid bars are used for this purpose, forcing the flange surfaces to be parallel. It has been found that the “no rotation” constraint has only a local influence on the deformed profile. The critical profile area where the transducers are located (in the mid section of the body), does not vary significantly whether the “no rotation” constraint is used or not [11] (not shown here).

The FEM calculations give in principle the change of position for every point of the meter body. Thus, the change of diameter in the horizontal and vertical directions and changes with respect to the transducer ports (i.e. inclination angles and directional orientation of the port (rotation, etc.)), are calculated. This includes the rotation around the vertical, axial and transversal axes, of the back plane of the transducer ports [14].

4 RESULTS AND DISCUSSION

The simulation results of the study are given in the present section. Finite element (FEM) calculations are shown in subsections 4.1 and 4.2, for a cylindrical pipe, a flanged pipe, and a flanged pipe with transducer ports (the full Q-Sonic 5 meter body). The wall thickness / inner radius ratio is w/R_0 = 0.25, and the pressure difference is ΔP_{mc} = (230 – 63) bar = 167 bar. Comparisons of the FEM results with the analytical calculation models described in subsection 3.3 are given in subsection 4.3.

4.1 Cylindrical (Straight) Pipe, and Flanged Pipe

FEM calculations for the cylindrical pipe are given in Fig. 4a, for 3 different boundary conditions: "ends free", "ends clamped" and "ends capped". The calculated radial displacement is relatively uniform along the pipe, ranging from about 74 µm, 70 µm to 66 µm, for the 3 types of boundary conditions, respectively.

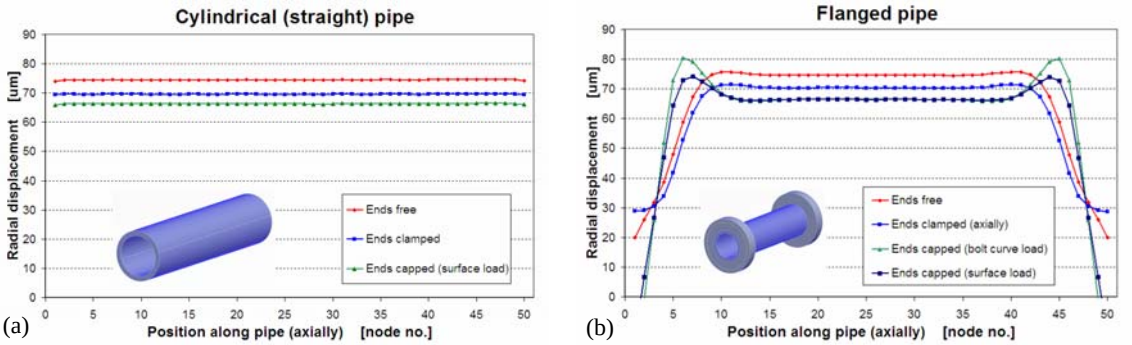

Fig. 4. Inner radius displacement of (a) a cylindrical pipe and (b) a flanged pipe, for ΔP_C = 167 bar and wall thickness / radius ratio w/R_0 = 0.25, calculated using finite element modelling (FEM).

Corresponding FEM calculations for the flanged pipe are given in Fig. 4b, for 4 different boundary conditions: "ends free", "ends clamped", "ends capped (bolt circle curve load)", and "ends capped (flange surface load)". The flanged pipe has the same dimensions as the Q-Sonic 5 meter body, and differs from the real meter body only by the absence of transducer ports. In all cases the radial displacement is highly non-uniform along the pipe, due to the flanges. This is also illustrated in Fig. 5. Of significant importance for the present study is the distribution of the radial displacement along the pipe. In the mid section of the pipe, outside the flange region (between nodes 10 and 40), the calculated radial displacement is relatively uniform along the pipe, ranging from about 75 µm, 70 µm to 67 and 67 µm, for the 4 types of boundary conditions, respectively. This is important, as this is the region in which the transducer ports and the acoustic paths are located.

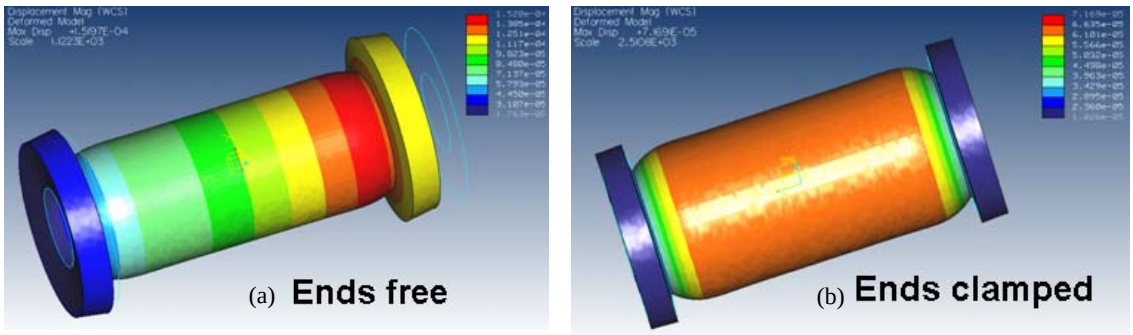

Fig. 5. FEM calculation of the pressure expansion of a flanged pipe with the same dimensions as the Ormen Lange Q-Sonic 5 meter body, for ΔP_{mc} = 167 bar and w/R_0 = 0.25. Boundary condition: (a) "ends free" and (b) "ends clamped"..

4.2 Flanged Pipe With Transducer Ports (Q-Sonic 5 Meter Body)

An example of a FEM calculation for the flanged pipe with transducer ports (the Ormen Lange Q-Sonic 5 meter body) is shown in Fig. 6, for the case of "ends free" boundary conditions. Due to the presence of the transducer ports, the radial displacement shows some asymmetry around the meter body, and to achieve representative quantitative figures for the radial displacement over the body, the radial displacement is calculated along four axial profile lines along the inner wall, denoted Line 1 (12 o'clock = 0°), Line 2 (9 o'clock = 270°), Line 3 (6 o'clock = 180°) and Line 4 (3 o'clock = 90°). FEM calculation results along these four lines are shown in Fig. 7, for 4 different boundary conditions: "ends free", "ends clamped", "ends capped (bolt circle curve load)", and "ends capped (flange surface load)".

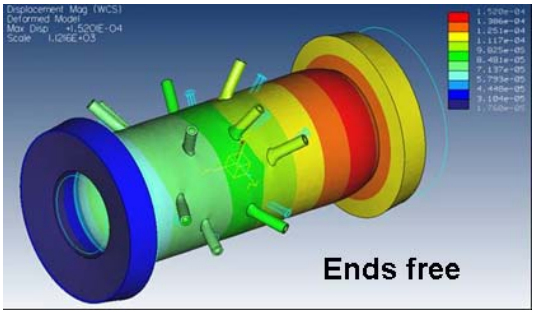

Fig. 6. FEM calculation of the pressure expansion of the Ormen Lange Q-Sonic 5 meter body, for ΔP = 167 bar and w/R = 0.25. Boundary condition: "ends free".

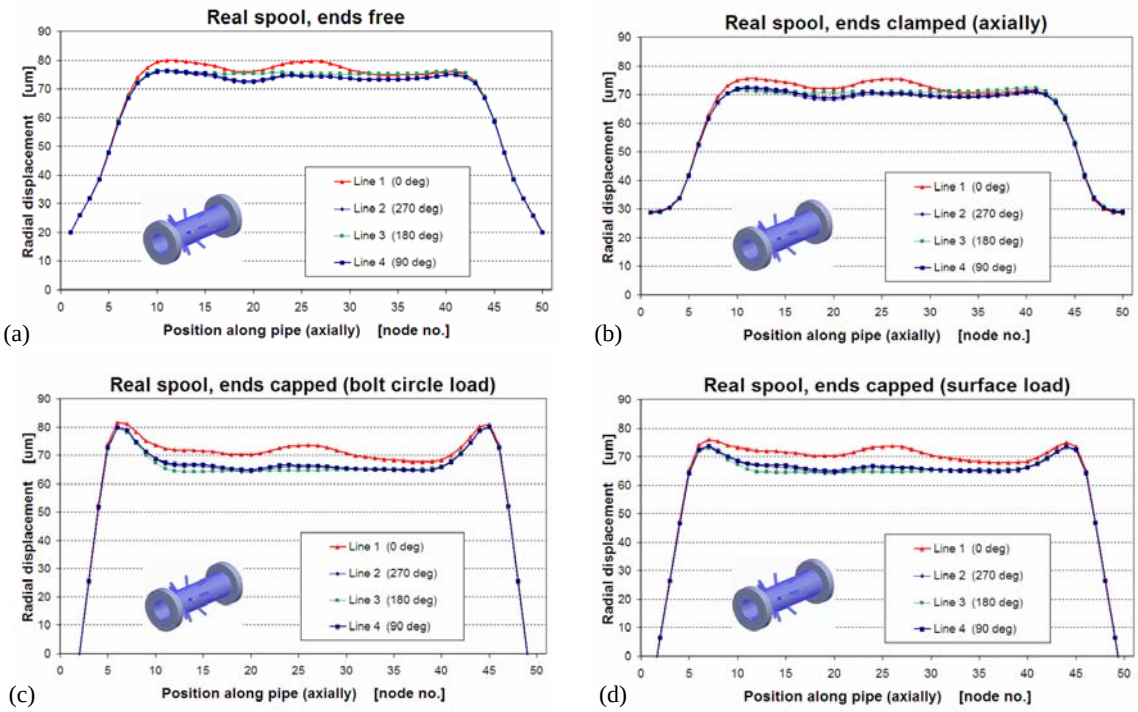

Fig. 7. Inner radius displacement of the Q-Sonic 5 meter body (with w/R_0 = 0.25) for ΔP_{mc} = 167 bar and different boundary conditions: (a) "ends free", (b) "ends clamped", (c) "ends capped (bolt circle curve load)" and (d) "ends capped (flange surface load)", calculated using FEM.

It is noted from Fig. 7 that the radial displacement is highly non-uniform along the pipe, similar to the flanged pipe in Fig. 4b. In the mid section of the pipe, outside the flange region (between nodes 10 and 40), the calculated radial displacement is relatively uniform along the pipe, but not as uniform as for the flanged pipe. This variation along the pipe is due to the presence of the transducer ports. The transducer ports are also responsible for the asymmetry observed around the pipe center axis. In the mid section of the pipe (between nodes 10 and 40), the calculated radial displacement ranges from about 64 μm to 80 μm, for the 4 profile lines and the 4 types of boundary conditions.

4.3 Comparison Of Results, With Discussion

The results shown in Sections 4.1 and 4.2 have been calculated for a wall thickness / inner radius ratio equal to w/R_0 = 0.25, as for the Ormen Lange Q-Sonic 5 meter body. Similar calculations have been made also for the ratios w/R_0 = 0.05, 0.10, 0.15 and 0.20, to (a) investigate the influence of wall thickness, w, on the behaviour of the meter body, (b) for comparison with analytical thin- and thick-wall theories, and (c) to establish a more general and representative data set as a basis for the conclusions of the study. All calculations have been made for a pressure change ΔP_{mc} = (230 – 63) bar = 167 bar (cf. Table 2).

It should be noted that in order to limit the simulation series and the number of parameters to be accounted for in the study, the flange thickness has been kept constant over the simulation series (that is, constant for all w/R_0), equal to the flange thickness of the full Ormen Lange Q-Sonic 5 meter body with w/R_0 = 0.25 [1,2]. In reality, a reduced wall thickness would of course be accompanied by a reduced flange thickness. However, the results obtained in the study, with a relatively wide "flat" mid section (cf. Figs. 4-7, and similar results for lower w/R_0, not shown here), indicate that this potential limitation does not seem to be a significant and important limitation of the study, and of minor importance for the conclusions.

Figs. 8, 9 and 10 show the inner radius displacement as a function of w/R_0, for the different calculation models (analytical and FEM) and "meter body geometries" (cylindrical pipe, flanged pipe, Q-Sonic-5 meter body), for different axial boundary conditions, "ends free", "ends clamped" and "ends capped", respectively. Parts (a) of the figures show the calculated inner radius displacement (ΔR) in mm, while parts (b) of Figs. 8 and 10 show the ratio of the calculated relative inner radius displacement ($\Delta R/R_0$) to the respective relative inner radius displacement of the thin-wall theory $(\Delta R/R_0)_{thinshell}$ (for the axial boundary condition in question). Only the absolute and relative radial changes, ΔR and $\Delta R/R_0$, are considered here[2].

Besides of the FEM calculations of the different meter body geometries, Figs. 8 and 10 also show calculations using the analytical thin-wall and thick-wall "Roark formulas" given in Table 4, for "ends free" and "ends capped" boundary conditions, respectively.

With respect to the FEM calculations of the different meter body geometries, the figures shown have been calculated as follows. For the cylindrical pipe, the radial displacement (as in Fig. 4a for w/R_0 = 0.25) has been averaged over the complete pipe length. For the flanged pipe, the radial displacement (as in Fig. 4b for w/R_0 = 0.25) has been averaged over the mid section of the pipe (nodes 10 to 40), since that is the region in which the transducer ports (and thus the acoustic paths) are located. (The regions close to the flanges are not of interest in that respect.) For the Q-Sonic 5 meter body (marked "flanged pipe, transd ports" in Figs. 8-10) the figures shown are calculated as follows. Firstly, for each axial profile line 1-4, the average displacement is calculated over the mid section of the line (nodes 10 to 40), for the same reason as for the flanged pipe (cf. Fig. 5 for w/R_0 = 0.25). Secondly, these average displacements for the 4 lines are averaged, to achieve a single number which represents the average radial displacement for the mid section of the Q-Sonic 5 meter body.

[2] The absolute and relative length changes, ΔL and $\Delta L/L_0$, have also been calculated (using the two analytical "Roark formulas" of Table 4 as well as FEM calculations for the three different "meter body geometries") (cf. [14]), but these results are not shown here.

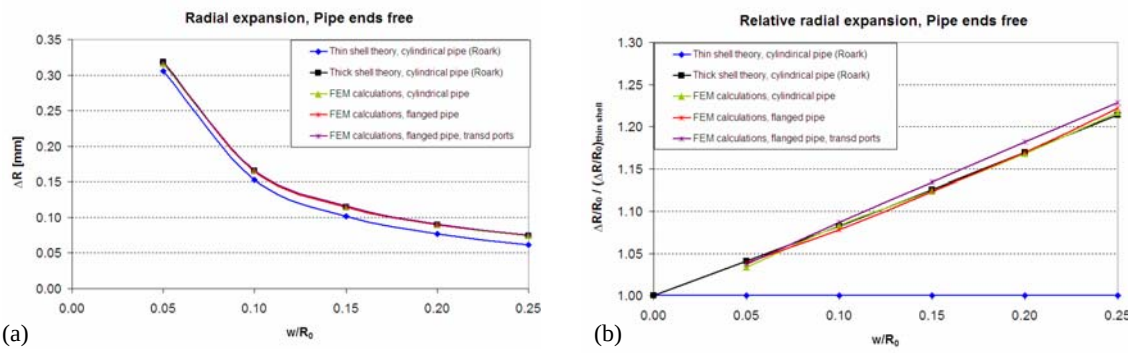

Fig. 8. Comparison of inner radius displacement obtained using different calculation models (the 2 cylindrical pipe models of Table 4 ("Roark formulas"), and 3 FEM calculations), for "ends free" boundary conditions, for ΔP_{mc} = 167 bar. (a) Inner radius displacement, and (b) inner radius displacement relative to the thin-shell theory (with "ends free" boundary conditions).

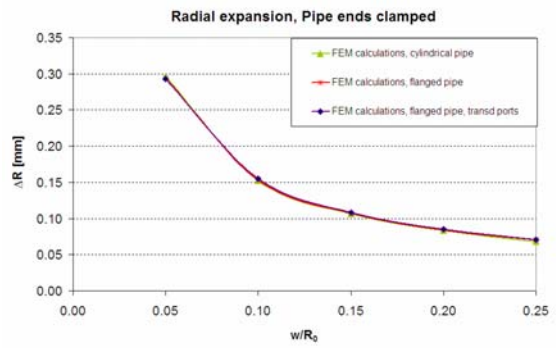

Fig. 9. Comparison of inner radius displacement (inner radius displacement) obtained using different calculation models (3 FEM), for "ends clamped" boundary conditions, for ΔP_{mc} = 167 bar. (Note that analytical models have not been available for this boundary condtion, cf. Table 4.)

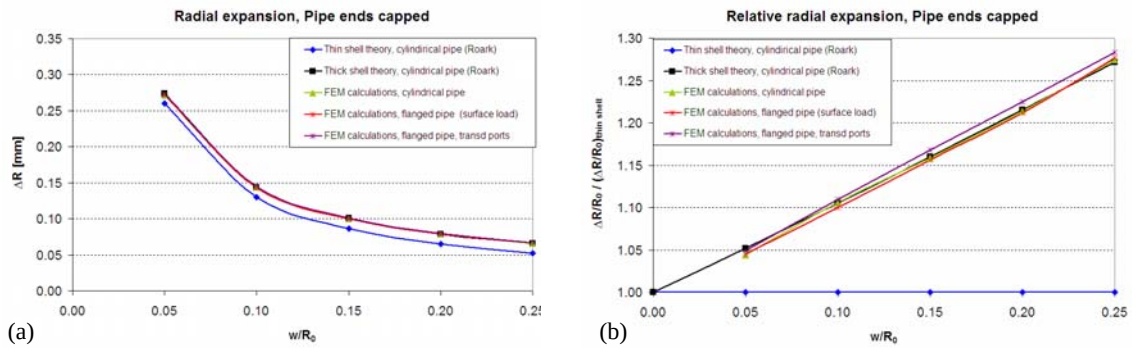

Fig. 10. Comparison of inner radius displacement obtained using different calculation models (the 2 cylindrical pipe models of Table 4 ("Roark formulas"), for "ends capped" boundary conditions, for ΔP_{mc} = 167 bar. (a) Inner radius displacement, and (b) inner radius displacement relative to the thin-shell theory (with "ends capped" boundary conditions).

First, consider parts (a) of Figs. 8-10, giving the absolute radial displacement (ΔR) in mm. It is noted that for the two types of axial boundary conditions for which analytical theories have been available, "ends free" and "ends capped" pipe constraints, the thin-shell models predict too low radial displacement, over the complete range of w/R_0 investigated, 0.05 to 0.25. From part (b) of Figs. 8 and 10, it follows that for w/R_0 = 0.1, the underestimation of the thin-shell models is about 8 and 10 % for the two boundary conditions, respectively, whereas for w/R_0 = 0.25, the underestimation is about 22 and 27 %, respectively.

The thick-shell models, however, are found to be in relatively close agreement with the FEM calculations for the cylindrical pipe. Moreover, the thick-shell models are in relatively close agreement also with the FEM calculations for the flanged pipe, and in fair agreement with the FEM calculations for the flanged pipe with transducer ports (the Q-Sonic 5 type of meter body). It appears that the radial displacement is slightly larger for the flanged pipe with transducer ports than for the cylindrical and flanged pipes, especially for large w/R_0. This is

ascribed to a reduced effective stiffness of the body wall due to the holes in wall caused by the transducer ports.

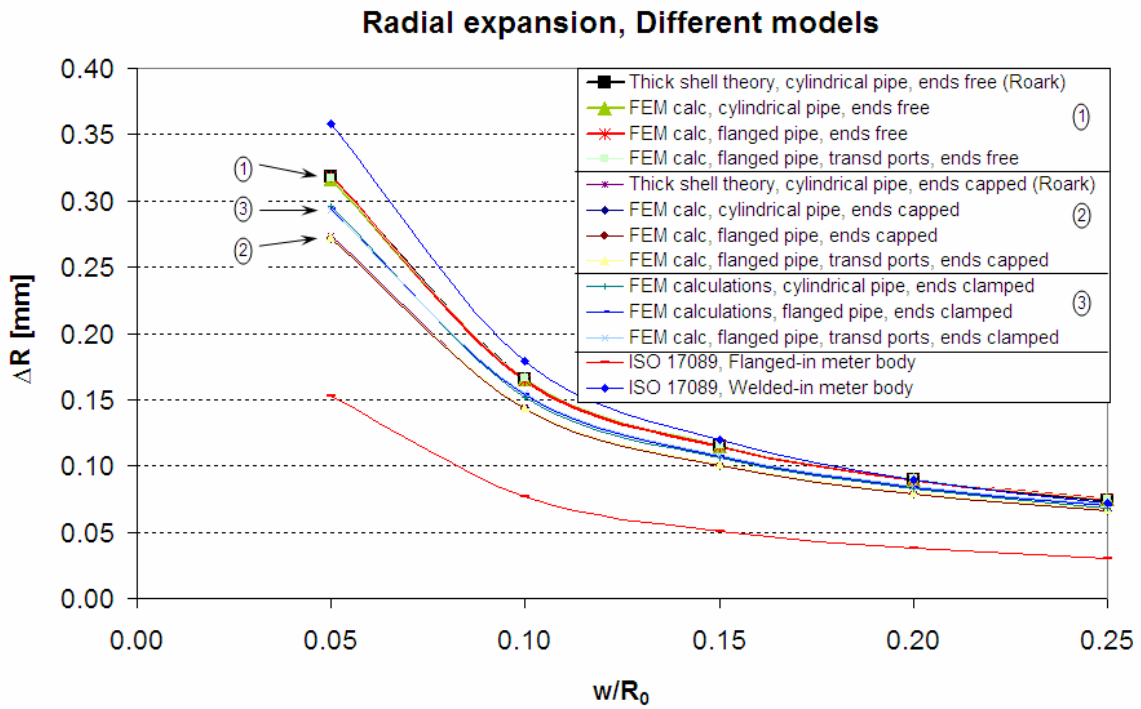

Fig. 11. Comparison of the radial displacement results shown in Figs. 7a, 8 and 9a (thin-shell model results excluded), with the 2 models used in ISO/CD 17089-1 (cf. Table 5).

From the above results, three important questions arise. Firstly, to what extent do the radial displacement results depend on the various boundary conditions? Secondly, how do these results compare with the results predicted by the ISO/CD 17089-1 models given in Table 5? And thirdly, what are the consequences for the volumetric flow rate measured by the USM?

Fig. 11 shows a comparison of the results given in of Figs. 8-10 (with the thin-shell model results excluded), together with the results predicted by the two ISO/CD 17089-1 models given in Table 5. It appears that the results are falling in five "groups", where the first three are indicated in the figure. Group nos. 1-3 contain the results for the "ends free", "ends capped" and "ends clamped" boundary conditions, respectively. Within each of these groups, there is a close agreement between the various calculations, as discussed above. For lower w/R_0, the three groups differ somewhat, whereas for w/R_0 approaching 0.25 the difference between the three groups becomes relatively small.

The other two "groups" in Fig. 11 are the ISO/CD 17089-1 model results. The "flanged-in meter body" model severely underestimates the radial displacement, whereas the "welded-in meter body" model gives results which at lower w/R_0 are higher than the other models, but becomes in agreement with groups 1–3 as w/R_0 approaches 0.25.

Fig. 12 shows the volumetric pressure correction factor, C_{psm}, calculated using the simplified model given by Eqs. (5)-(6), which is strictly valid only for USM inclination angles equal to 45°. We find the same type of "grouping" and model behaviour as described above for the radial displacement isolated, in Fig. 11. It should be noted, however, that C_{psm} accounts for effects of both (A) the radial displacement (the change of cross-sectional area) and (B) the change of ultrasonic path geometry (due to the movement of the transducer ports), as discussed in Section 3.3.

From Eq. (5), the (percentage) influence of these two factors (A) and (B) on the volumetric flow rate measurement, Q, is given as $(C_{psm}-1)*100\%$ (still according to the simplified model, however, with inclination angles equal to 45°). These types of result are shown in Fig. 13, for the various calculation models and "meter body geometries" discussed in the present paper.

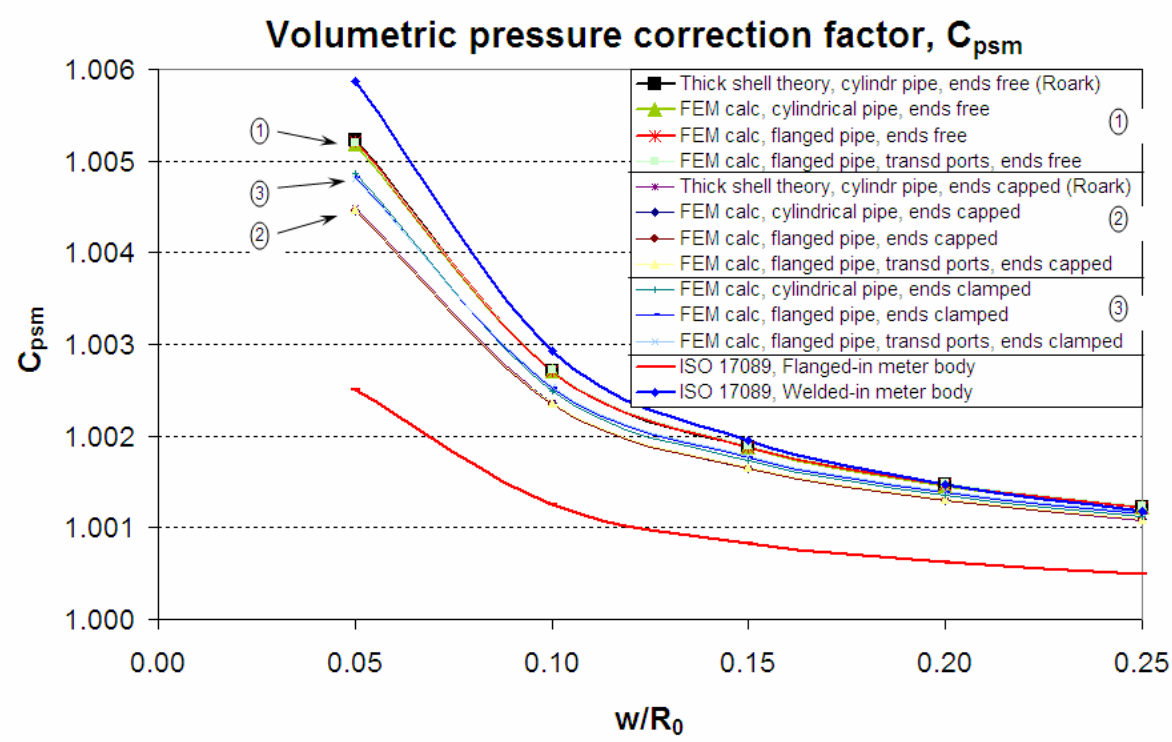

Fig. 12. Volumetric pressure correction factor, C_{psm}, for the Q-Sonic 5 meter body, calculated using different models, as a function of wall thickness – inner radius ratio.

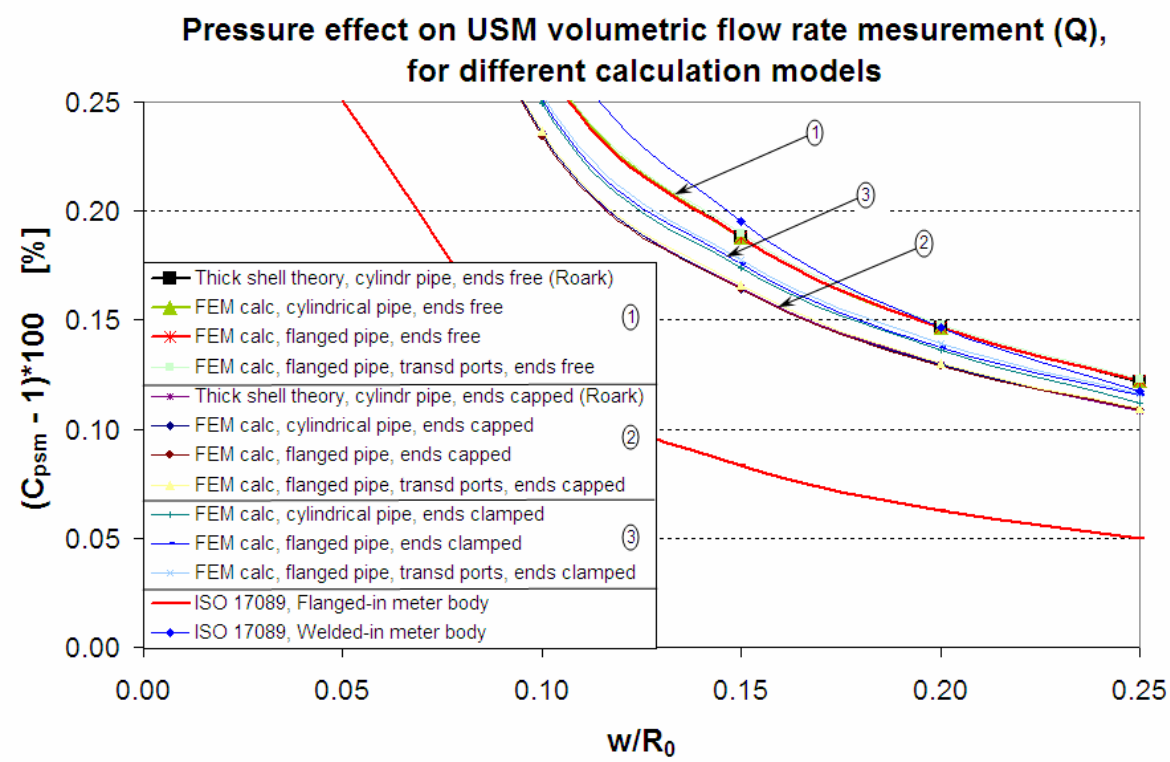

Fig. 13. Pressure effect on USM volumetric flow rate measurement (Q) for the Q-Sonic 5 meter body, calculated using different models, as a function of wall thickness – inner radius ratio.

Again, the results fall into five groups, where the first three are indicated in the figure, for the "ends free", "ends capped" and "ends clamped" boundary conditions, respectively. Within each of these groups, there is also here a good agreement between the various calculations.

For w/R_0 approaching 0.25 the difference between the three groups becomes relatively small, but not negligible. For the Ormen Lange meter, with w/R_0 = 0.25, the pressure effect is calculate to be about (0.12 ± 0.01) %, where the indicated "uncertainty" accounts for the deviation between groups 1-3 only. That is, if an "uncertainty" of 0.01 % is acceptable for the Ormen Lange project, the actual axial boundary condition being used ("ends free", "ends capped" and "ends clamped") should not be critical for calculation of the radial displacement and the pressure correction factor.

Fig. 13 also shows the ISO/CD 17089-1 model results. The "flanged-in meter body" model provides a severe underestimation, and is not recommended. The "welded-in meter body" model, on the other hand, gives results which for w/R_0 approaching 0.25, becomes in agreement with the groups 1–3.

However, on background of the general pattern apparent in the above results, both of the thick-shell models given in Table 4 ("Roark formulas", for "ends free" and "ends capped" boundary conditions) seem to provide more representative results than the "welded-in meter body" model given in Table 5. This is so for cylindrical pipes, flanged pipes as well as for flanged pipes with transducer ports (the Q-Sonic 5 meter body), and for all three types of axial boundary conditions considered, "ends free", "ends capped" and "ends clamped". The Roark thick shell models also have the advantage that they are derived mathematically from physical principles, and account for both radial and length changes of the pipe.

5 SUMMARY AND CONCLUSIONS

In [1,2] (for Phase 1 of the study) correction factors were proposed for P & T effects on the 18" Q-Sonic 5 ultrasonic flow meters, from Westerbork flow calibration conditions (63 barg and 7 °C) to Ormen Lange line conditions (nominally at 230 barg and 40 °C). The proposed correction factors account for several P & T effects, such as

(A) Change of the meter's cross-sectional area,
(B) Change of the ultrasonic path geometry (inclination angles and lateral chord positions),
(C) Change of the length of the ultrasonic transducer ports,
(D) Change of the length of the ultrasonic transducers,
(E) Change of the Reynolds number.

For the Ormen Lange application, it was shown in [1,2] that evaluation of all of the effects (A) – (E) have been necessary to evaluate the effect of pressure and temperature on the meter.

In the present paper, under Phase 2 of the study, pressure effects on the meter body related to the effects (A) and (B) have been revisited and analysed in more detail, for three different "meter body geometries",

- cylindrical (straight) pipe,
- flanged pipe,
- flanged pipe with ultrasonic transducer ports (the Ormen Lange Q-Sonic 5 meter body),

with respect to

- influence of axial boundary conditions ("ends free", "ends clamped", "ends capped"), and
- influence of meter body wall thickness.

A combination of finite element modelling (FEM) and analytical modelling has been used for this purpose. Meter body wall thicknesses in the range w/R_0 = 0.05 - 0.25 have been studied.

It has been found that with respect to pressure effects on the inner radius displacement, the cylindrical pipe thick-shell model with either "ends free" or "ends capped" axial boundary conditions (cf. the "Roark formulas", cf. Table 4) provides a good approximation for all three "meter body geometries" considered here (cylindrical pipe, flanged pipe, and flanged pipe with ultrasonic transducer ports), for wall thicknesses up to w/R_0 = 0.25.

The thin-shell models (cf. the "Roark formulas", cf. Table 4) represent relatively poor approximations in the range w/R_0 = 0.05 - 0.25. Since the complexities in implementation of the thick- and thin-shell models are similar, the thick-shell model should in general be preferred, due to its significantly higher accuracy.

It may thus be preferable to use one of the thick shell models for calculation of the "instantaneous P&T correction factor" for the Ormen Lange meter. Since this factor is to account for the small excess gas pressure relative to the nominal pressure of 230 barg only (i.e. a few bars), the results using the Roark thin- and thick shell models may not deviate much. However, by using the more accurate thick shell model, discussions in relation to this point may be avoided.

The results are compared with two models used in ISO/CD 17089-1, the "flanged-in meter body" and the "welded-in meter body" models [6], cf. Table 5. The "flanged-in meter body" model provides a severe underestimation, and is not recommended. The reason for the underestimation using this model is expected to be the fact that the mid section of the USM (in which the transducer ports and the acoustic paths are located) expands relatively uniformly with pressure, which possibly violates the pressure expansion assumption underlying the "flanged-in meter body" model.

The "welded-in meter body" model [6] yields results which for w/R_0 close to 0.25 are in close agreement with the results using the Roark thick-shell and FE models. However, in general the results demonstrate that the two thick-shell models (the "Roark formulas", cf. Table 4) provide more representative results than the "welded-in meter body" model. This is so for cylindrical pipes, flanged pipes as well as for flanged pipes with transducer ports (including the Q-Sonic 5 meter body), and for all three types of axial boundary conditions considered, "ends free", "ends capped" and "ends clamped". Both of the thick-shell models may thus be preferred as compared with the "welded-in meter body" model, for all cases mentioned above.

It has been shown here that for the Ormen Lange project, the actual axial boundary condition being used ("ends free", "ends clamped" or "ends capped") is not critical for calculation of the radial displacement and the pressure correction factor. That is, the boundary conditions approach taken in [1,2], where the "ends free" boundary condition was used, should be a valid and relatively accurate approach. For the Ormen Lange meter, the uncertainty of the volumetric flow rate measurement due to the choice of axial boundary condition made in the calculation of the "nominal P&T correction factor", is estimated to about ±0.01 %.

The implications of the results reported here with respect to the "nominal P&T correction factor" and the "instantaneous P&T correction factor" proposed in [1,2], will be documented and reported in an unclassified technical report, to be available early 2009, at the completion of the ongoing Phase 2 of the project [14].

SYMBOL NOTATION

P_0 : gas pressure at "dry calibration" conditions (taken to be 1 atm. = 101325 Pa)

P_c : gas pressure at flow calibration (Westerbork) conditions [Pa]

P_m : gas pressure at operating (Ormen Lange) conditons [Pa]

ΔP_{mc} : change of gas pressure from flow calibration (Westerbork) to operating (Ormen Lange) conditons [m]

T_0 : gas temperature at "dry calibration" conditions (taken to be 20 ^oC)

T_c : gas temperature at flow calibration (Westerbork) conditions [^oC]

T_m : gas temperature at operating (Ormen Lange) conditons [^oC]

ΔT_{mc} : change of gas temperature from flow calibration (Westerbork) to operating (Ormen Lange) conditons [m]

R_0 : inner radius of USM meter body at "dry calibration" conditions (taken as 1 atm. and 20 ^oC) [m]

R_c : inner radius of USM meter body, at flow calibration (Westerbork) conditions [m]

R : inner radius of USM meter body, at operating (Ormen Lange) conditions [m]

ΔR : change of inner radius of USM meter body, from flow calibration (Westerbork) to operating (Ormen Lange) conditons = $R - R_c$ [m]

L_0 : length of USM meter body, at "dry calibration" conditions (taken as 1 atm. and 20 ^oC) [m]

ΔL : change of length of USM meter body, from flow calibration (Westerbork) to operating (Ormen Lange) conditons [m]

w : wall thickness of USM meter body, at "dry calibration" conditions (taken to be 1 atm. and 20 ^oC) [m]

Y : Young's modulus for the meter body material [Pa]

σ : Poisson's ratio for the meter body material [-]

α : coefficient of linear thermal expansion of the meter body material [K^{-1}]

β : radial linear pressure expansion coefficient of the meter body [Pa^{-1}]

β^* : axial (length) linear pressure expansion coefficient of the meter body [Pa^{-1}]

K_T : radial temperature correction factor for the USM meter body [-]

K_P : radial pressure correction factor for the USM meter body [-]

C_{tsm} : volumetric temperature correction factor for the USM meter body [-]

C_{psm} : volumetric pressure correction factor for the USM meter body [-]

q : corrected volumetric flow rate at line (Ormen Lange) conditions [m^3/s]

q_{USM} : volumetric flow rate output from the USM at line (Ormen Lange) conditions [m^3/s]

$q_{USM,c}$: volumetric flow rate output from the USM at flow calibration (Westerbork) conditions [m^3/s]

N : number of acoustic paths in the USM [-]

w_i : integration weight factor for acoustic path no. i of the USM [-]

L_i : interrogation length for path no. i, at operating (Ormen Lange) conditions [m]

y_i : lateral distance from the pipe center (lateral chord position) for path no. i, at operating (Ormen Lange) conditions [m]

ϕ_i : inclination angle (relative to the pipe axis) of path no. i, at operating (Ormen Lange) conditions [radians]

y_{ic} : lateral distance from the pipe center (lateral chord position) for path no. i, at flow calibration (Westerbork) conditions [m]

ϕ_{ic} : inclination angle (relative to the pipe axis) of path no. i, at flow calibration (Westerbork) conditions [radians]

t_{1i} , t_{2i} : measured transit times for upstream and downstream sound propagation of path no. i [s]

$N_{refl,i}$: number of wall reflections for path no. i ($N_{refl,i}$ = 0, 1 or 2 in current USMs), i = 1, …, N [-]

ACKNOWLEDGEMENTS

The authors wish to thank the Ormen Lange partners for the possibility to publish the present paper. Comments given in discussions with the Ormen Lange project (in particular StatoilHydro and Shell representatives) and the Norwegian Petroleum Directorate (NPD) have been of great value to the study.

REFERENCES

[1] **P. Lunde, and K.-E. Frøysa**, "Ormen Lange ultrasonic gas flow meters. A study for establishment of corrections for pressure and temperature effects", CMR report no. CMR-06-A10048-RA-01, Christian Michelsen Research AS, Norway (March 2007).

[2] **P. Lunde, K.-E. Frøysa and T. Folkestad**, "Pressure and temperature effects for Ormen Lange ultrasonic gas flow meters", Proc. of *25th International North Sea Flow Measurement Workshop, Oslo, Norway, 16-19 October 2007.*

[3] **R.J. Whitson**, "Review of report: "Ormen Lange ultrasonic gas flow meters. A study for establishment of corrections for pressure and temperature effects"", Report no. 2007/290, TUV-NEL Ltd., Glasgow, Scotland (December 2007).

[4] Elster-Instromet Q-Sonic 5 ultrasonic flow meter web site, Elster-Instromet NV, Rijkmakerlaan 9, B-2910 Essen, Belgium (2006); http://www.elster-instromet.com/en/ultrasonic_flow_metering.html

[5] **W. C. Young and W. C. Budynas**, *Roark's formulas for stress and strain*, 7th edition (McGraw-Hill, New York, 2001).

[6] "Measurement of flow in closed conduits – ultrasonic meters for gas – Part 1: meters for custody transfer and allocation measurement", ISO/CD 17089-1, August 31, 2007, International Organization for Standardization, Genéve, Switzerland. (Committee Draft.) (Reference number ISO/TC 30/SC 05 N210.)

[7] "GERG project on ultrasonic gas flow meters, Phase II", edited by Lunde, P., Frøysa, K.-E. and Vestrheim, M., GERG TM11 2000, Groupe Européen de Recherches Gazières (VDI Verlag, Düsseldorf, 2000).

[8] **Lunde, P. and Frøysa, K.-E.:** "Handbook of uncertainty calculations. Ultrasonic fiscal gas metering stations". Handbook prepared on behalf of the Norwegian Society of Oil and Gas Measurement (NFOGM) and the Norwegian Petroleum Directorate (NPD) (December 2001), 279 p. (ISBN 82-566-1009-3). (Free download available from www.nfogm.no.)

[9] "Manual of petroleum measurement standards. Chapter 12 - Calculation of petroleum quantities. Section 2 - Calculation of liquid petroleum quantites measured by turbine or displacement meters", First edition. American Petroleum Institute, U.S.A. (September 1981). (Paragraphs 12.2.5.1 and 12.2.5.2.)

[10] "Manual of petroleum measurement standards. Chapter 12 - Calculation of petroleum quantities. Section 2 - Calculation of liquid petroleum quantites using dynamic measurement methods and volumetric correction factors. Part 1 - Introduction", Second edition. American Petroleum Institute, Washington D.C., U.S.A. (May 1995). (Paragraphs 1.11.2.1 and 1.11.2.2.)

[11] "Institute of Petroleum. Petroleum Measurement Manual. Part X - Meter Proving. Section 3 - Code of practice for the design, installation and calibration of pipe provers", Published on behalf of The Institute of Petroleum, London (J. Wiley & Sons, Chichester, 1989), Section 10.7, p. 31 (ISBN 0 471 92231 5).

[12] "Measurement of gas by ultrasonic meters", A.G.A. Report no. 9, American Gas Association, Transmission Measurement Committee (June 1998).

[13] **V. Martinez**, "Spool deformations. FEM analysis", CMR Prototech Report no. RP-30363-PR-01, CMR Prototech, Bergen Norway (August 2008).

[14] **P. Lunde, and K.-E. Frøysa**, "Ormen Lange ultrasonic gas flow meters. A study for establishment of corrections for pressure and temperature effects. Phase 2", CMR report, Christian Michelsen Research AS, Norway (in preparation).

North Sea FLOW Measurement Workshop

Paper 6.2

A General Methodology for Geometry Related Pressure and Temperature Corrections in Ultrasonic Time for Flight Flowmeters

Richard J. Whitson
TUV NEL

TÜV SÜD

nel technology for life

A General Methodology for Geometry Related Pressure and Temperature Corrections in Ultrasonic Time-of-Flight Flowmeters

Richard J. Whitson, TUV NEL

1 INTRODUCTION

Ultrasonic flowmeters (USFM) are often operated at pressure and temperature conditions that are different from the pressure and temperature conditions under which the static (dry) or dynamic (wet) calibration was carried out. During dynamic calibration, the systematic errors are brought to zero by determining and then applying the meter flow calibration factor. The meter's reference conditions then become those of the dynamic calibration. Any subsequent change in temperature or pressure will alter the physical dimensions of the meter and, if not corrected for, will introduce a systematic flow measurement error.

Recent work ([1], [2]), has drawn attention to the lack of consistency and traceability between International Standards [3] and Industry practice ([4], [5]) as to how to deal with calculation or estimation of this type of systematic error in a manner that is suitable for a range of types of USFM. Whilst occasional references to background work such as [6] are made, that work is typically restricted to a narrow range of application or type of meter body and care needs to be exercised in drawing general conclusions to the importance of these systematic effects in a wider context. This lack of consistency and traceability is understandable given that accuracy requirements have moved on since many of those standards and practices were originally conceived when perhaps 1% error was an acceptable goal for USFMs. However, due to improvement and development in USFM technology and extension of its areas of application, the demand at fiscal metering level is now for correction of any systematic errors greater than 0.1%. Hence there is a need for clarity, consistency and tracability in how these corrections are calculated.

In the course of executing work [7] sponsored by the Norwegian Petroleum Directorate (NPD), the basis of a methodology for direct calculation of these systematic errors was developed as a means of checking the results of a Finite Element (FE) modelling project [1], [2]. That basic methodology uses the fundamental equations of Roark [8] and has subsequently undergone significant further development and simplification into the process described in this paper.

The method can be used on its own or if the meter body is complex in shape, to supplement or check the results of FE analysis and is now scheduled for inclusion in the forthcoming release of ISO 17089-1 [9] and in a simplified form in the planned revision to BS 7965 [3].

2 THE METHODOLOGY

2.1 General Approach and Background

In the following Sections 2.2 through 2.5, a simple and quick approach is given to allow an initial estimate to be made of the flow error caused by temperature and pressure conditions that differ from the calibration reference condition. If this error is significant relative to the uncertainty required for the particular class of meter being considered, a more detailed calculation can be performed as described in Section 2.6 to obtain a more precise value for the flow error. Annex A provides a more in-depth explanation of the detailed calculation process and its background as well as a worked example.

The process provides a method of estimating the systematic errors due to meter geometry changes regardless of the particular type, make or model of time-of-flight spool meter or of the fluid being used. The methodology does not however apply to clamp-on USFMs such as

those in BS 8452 [10] since these will generally measure pipe diameter and wall thickness under actual operating conditions.

A simple time-of-flight layout is shown in Fig.1. For any given path, the indicated flow can be written in the following standard form in terms of the meter internal diameter, D, the path-length, L, and the transducer axial separation, X, rather than path angle, ϕ:

$$Q = A.v = \frac{\pi D^2}{4}\frac{L^2}{2X}\left(\frac{1}{t_{AB}} - \frac{1}{t_{BA}}\right) \qquad (1)$$

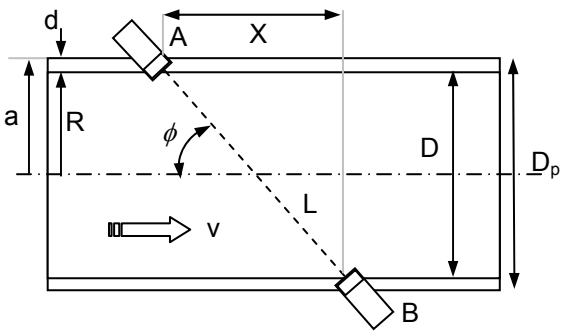

Fig. 1 - Basic time-of-flight setup

For the simple meter arrangement shown in Fig.1, X is obtained from simple trigonometry as X = L.cosϕ

Geometry change causes two primary effects:

- It changes the actual acoustic path length and path angle between a given transducer pair and consequently, if uncorrected, introduces a path velocity error and hence gives rise to a flow error.
- Any diameter change will result in an area change and, if ignored, will introduce a further flow error.

Using equation (1), the ratio between Q_0 at a reference calibration condition and Q_1 at different conditions can be written as a flow correction factor [4], Q_1/Q_0, given by:

$$\frac{Q_1}{Q_0} = \left(\frac{D_1}{D_0}\right)^2 \left(\frac{L_1}{L_0}\right)^2 \left(\frac{X_0}{X_1}\right) \qquad (2)$$

This form is useful since it separates the flow area effect, D^2, from the path-length effect, L^2, from the axial extension effect (or path angle effect), X.

Alternatively, the equivalent form to (2) but expressed as a relative flow error, $\Delta Q/Q$, can be used:

$$\frac{\Delta Q_{1,0}}{Q_0} = \frac{Q_1}{Q_0} - 1 \qquad (3)$$

Temperature and pressure are independent effects that need to be evaluated separately and both effects need to be taken into account for a given situation. The respective effects can work either in the same direction or in opposition to each other. For example, a pressure increase associated with a temperature decrease will partly cancel each other whilst a pressure increase in combination with a temperature increase (or pressure reduction in association with a temperature reduction) will reinforce the correction effect needed.

In a multi-path flowmeter, the effect has to be calculated for each of the individual paths and the effect on total flow obtained after integrating the flows once the path-weighting factors have been applied.

As described in Annex A, Section A.1, the geometry-related correction calculations can either be carried out as a single-stage or a three-stage calculation. A single-stage is preferred for the initial estimate.

2.2 Correction For The Body Temperature Change

For all meter types, the geometry-related temperature correction for the effect of a temperature difference, ΔT, can be given as a straightforward analytical solution related to the material thermal expansion constant and is relatively easy to account for since it expands the dimensions according to:

$$\begin{aligned} L_1 &= L_0(1+\alpha.\Delta T) \\ X_1 &= X_0(1+\alpha.\Delta T) \\ D_1 &= D_0(1+\alpha.\Delta T) \end{aligned} \tag{4}$$

Using equation (2), the flow correction factor due to a body temperature change is therefore given by:

$$\frac{Q_1}{Q_0} = (1+\alpha.\Delta T)^3 = \left(1+3.\alpha.\Delta T+3.(\alpha.\Delta T)^2+(\alpha.\Delta T)^3\right) \tag{5}$$

Other than in extreme situations, $\alpha.\Delta T$ is generally very small and equation (5) can be simplified to:

$$\left(\frac{Q_1}{Q_0}\right)_{bodytemperature} = 1+3.\alpha.\Delta T \tag{6}$$

Or alternatively, expressed as a flow error:

$$\left(\frac{\Delta Q}{Q}\right)_{bodytemperature} = 3.\alpha.\Delta T \tag{7}$$

Table 1 gives typical values of thermal expansion coefficient for common body materials and Fig.2 shows a graphical presentation of equation (7) for two of those materials.

Table 1 — Common Thermal Expansion Coefficients in the 0 - 100°C range

Material	α (m/m°C)
Carbon Steel	$12 \cdot 10^{-6}$
Stainless Steel (Austenitic)	$10 \cdot 10^{-6}$
Stainless Steel (Ferritic)	$13 \cdot 10^{-6}$

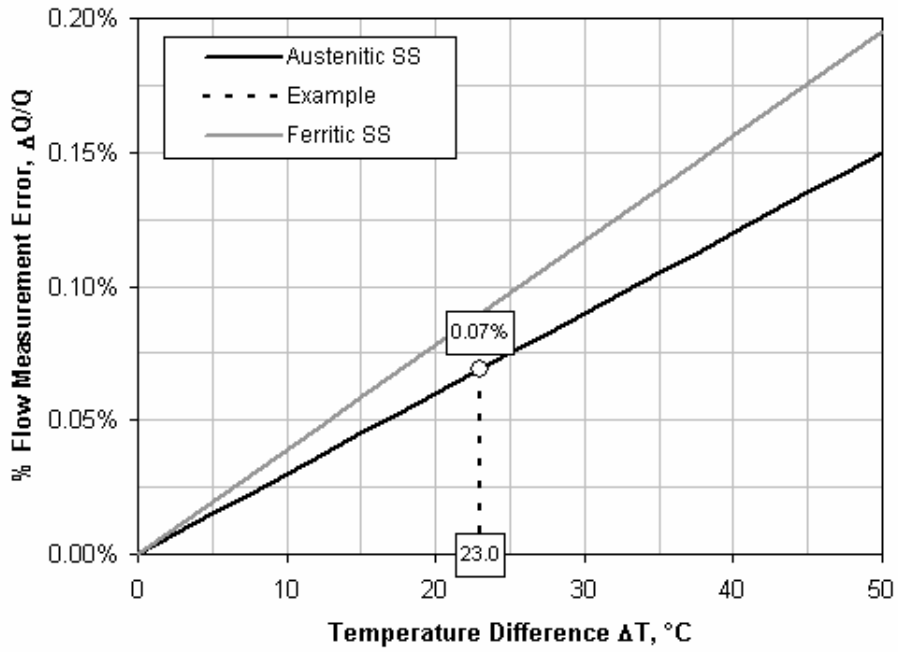

Fig. 2 - Temperature related flow error for two example material types

Fig.2 can be used to quickly estimate the percentage correction required for a given temperature change. The example point for a 23°C temperature change with an Austenitic Stainless Steel body shows a 0.07% correction. If ΔT is positive, $\Delta Q/Q$ will be positive and the meter will under-read the flow by the indicated amount. If ΔT is negative, $\Delta Q/Q$ will be negative, i.e. the meter will over-read the flow.

For large temperature differences, for example in cryogenic applications, it is recommended that the more exact form of temperature correction given by equation (5) is used in preference to the simplified version of equation (7).

2.3 Initial Estimate For The Body Pressure Correction

The geometry related pressure correction is complex and depends on the design of the meter body, its end connections and the way the meter ends are supported in operation.

The equations of Roark [8] for generally cylindrical bodies are used as the basis of the analysis. These have for many years been taken as the fundamental basis for stress analysis of pressure vessels and are derivations from the basic Lamé-Clapeyron equations of 1833. Annex A, Section A.2 gives the detailed derivations used.

In the present USFM market, the various meter designs offered can be grouped into three broad categories:

- Welded-in cylindrical body designs
- Meter bodies consisting of a pipe with welded-on flanges
- Non cylindrical meter body designs, for example those based on casting

The following sub-sections provide a means of making an initial estimate of the pressure related flow error for any body type.

2.3.1 Initial simple estimate for any body type

As a first stage in estimating the pressure effects, a general basic expression can be derived assuming the meter body consists simply of a cylindrical pipe. An estimate of the maximum expected flow error due to a body pressure change, ΔP, is (as described in Annex A, section A.7) given by:

$$\left(\frac{\Delta Q}{Q}\right)_{bodypressure,\max imum} = 4\cdot\frac{\Delta R}{R} = 4\cdot\left(\frac{a^2+R^2}{a^2-R^2}+\sigma\right)\cdot\frac{\Delta P}{E} \qquad (8)$$

If the meter body is irregular or non-cylindrical (for example as might be the case for a cast body), then for the purposes of this initial estimate the value of outside radius, a, should be taken as the point where the wall is thinnest since this will give the largest estimate of flow error.

Equation (8) can be presented in graphical form as shown in Fig.3 for a range of values of d/R, i.e. the ratio of wall thickness to internal radius d/R = (a-R)/R = (a/R)-1, and provides a rapid means of estimating the maximum expected flow error due to body pressure changes.

The figure is plotted for a body material with Young's Modulus of $2*10^{11}$ N/m^2 and a Poison's Ratio of 0.3. The example of a 63 bar ΔP shows the maximum expected pressure induced error to be 0.06% for a d/R = 0.25. If ΔP is negative, ΔQ/Q will be negative (i.e. the meter will over-read the flow).

Since equation (8) and Fig.3 provide a maximum expected error, the reader can if they desire, go straight to Section 2.5 (taking $K_E = K_S = 1$) to assess the significance of the error without the need of the refinement in the initial estimate provided in the following Sections 2.3.2 and 2.3.3 since these will result in a lower value for the flow error.

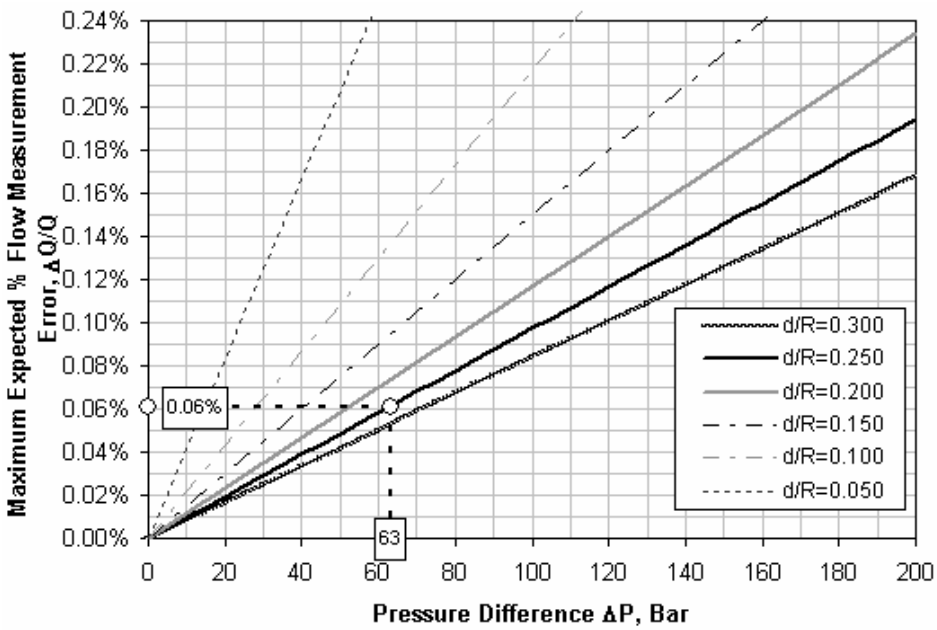

Fig. 3 - Maximum expected pressure related flow error for different d/R ratios

2.3.2 Refinement in initial estimate to account for different meter body designs

Flanged ends or irregular shape to the body will stiffen the body compared to the simple cylindrical pipe approach used in Section 2.3.1. Consequently, the body expansion and resulting flow error will be less than that given by equation (8) and Fig.3. To compensate for this local stiffening effect a body "style correction factor", K_S, is used to give a revised estimate of the flow error:

$$\left(\frac{\Delta Q}{Q}\right)_{bodypressure,rev1} = K_S\left(\frac{\Delta Q}{Q}\right)_{bodypressure,\max imum} \qquad (9)$$

K_S will always be less than or equal to 1. The value of K_S to be used for a given body type is as follows:

- For a welded-in body with no flanges within 1.D_P of the ultrasonic transducer locations, K_S = 1, i.e. the meter body behaves as a simple pipe.
- For a flanged meter body (for example, consisting of two flanges welded to a pipe), or welded-in design where neighboring flanges are within 1.D_P of the transducer positions, the value of K_S has to be calculated as described in Annex A, sections A.3.
- For irregularly shaped meter bodies, for example cast bodies, K_S is obtained as follows based on an average flow error:

    i. Equation (8), or Fig.3, is used to obtain a 2nd flow error, y, but this time based on the thickest wall section.

    ii. K_S is then calculated as, K_S = 0.5 (1+ y/x) where x = the initial estimate based on the thinnest wall section.

2.3.3 Refinement in initial estimate for effects of end loading and end support or constraint

Equation (8) and Fig.3 are based on the worst case conditions for radial body expansion (no end loads and free-ends). The effect of the best case conditions (pressure end loads and free ends) for minimal radial body expansion can be taken into account by introducing an "end correction factor", K_E, given in Fig.4 (for a poison's ratio = 0.3).

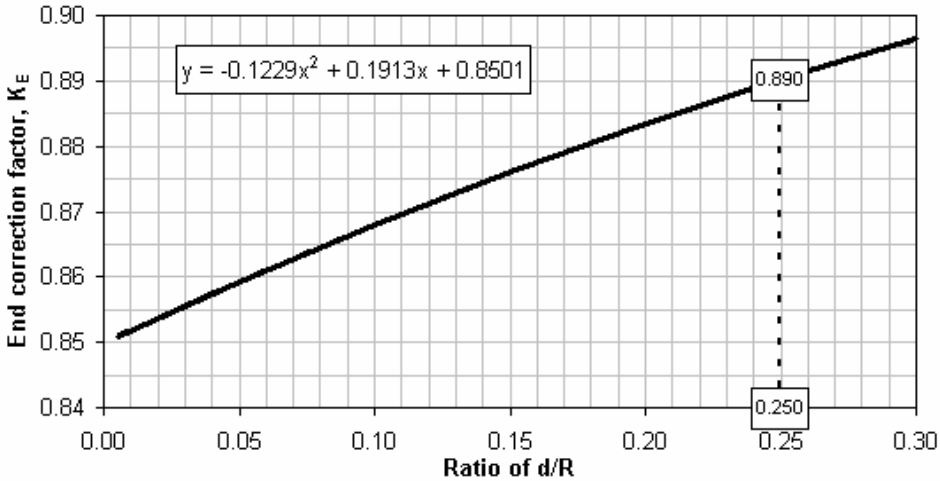

Fig. 4 - End loading and support correction factor K_E

This is derived simply from the ratio of equations (A.5) and (A.7) in Annex A. In the example in Fig.4, K_E = 0.89 for a d/R ratio = 0.25. Note that the smallest value K_E can have is 0.85.

The combined flow error ΔQ/Q then becomes:

$$\left(\frac{\Delta Q}{Q}\right)_{bodypressure} = K_E \cdot K_S \left(\frac{\Delta Q}{Q}\right)_{bodypressure,\max imum} \tag{10}$$

Note, equation (10) gives an estimate of the expected minimum flow error. It can therefore be used in combination with the maximum flow error (i.e. with K_E = K_S = 1) to provide an initial estimate of the range or tolerance in expected flow error.

2.4 Effects 0f Transducer Ports

The combined impact of the transducer and the transducer port are normally an order of magnitude smaller than the effect on the meter body and can be neglected for most cases. Any effects due to the speed of sound dependence of the recess are neglected for the purposes of this method. However, for reference, Annex A, Section A.5 provides a simple

calculation method that includes an estimate of port effects. The transducer material coefficients have to be known and for these the manufacturer should be consulted.

2.5 Total Metering Error

The initial estimate of the combined flow error due to a temperature and a pressure difference is given by:

$$\left(\frac{\Delta Q}{Q}\right)_{combined,estimate} = \left(\frac{\Delta Q}{Q}\right)_{bodytemperature} + K_E \cdot K_S \cdot \left(\frac{\Delta Q}{Q}\right)_{bodypressure,\max imum} \quad (11)$$

Table 2 provides suggested values as an aid to deciding whether a particular systematic error is significant or not for particular classes of gas meter.

If the flow error is judged insignificant then it can be dismissed and no further calculation needed.

If the flow error is deemed to be significant and hence requires correction, the detailed calculation as described in Section 2.6 can be performed to obtain a more precise flow correction factor. Note: If calculations in Sections 2.3.2 and 2.3.3 were omitted in the estimate for pressure effect, a repeat estimate can be performed using those sections to provide a lowered estimate before reassessing the need for the more detailed calculation.

Table 2 — USM Classifications and Suggested Systematic Error Significance

Meter Class	Typical Application	Typical volume flow rate uncertainty (from BS 7965) at 95% confidence level	Suggested level of significant systematic error
1	Custody transfer	< 0.7 %	0.1 %
2	Allocation metering	< 1.5 %	0.2 %
3	Utilities/fuel gas	< 3.0%	0.4 %
4	Process/flare gas	< 7.5%	1 %

2.6 Detailed Calculation Procedure

Sections A.2 through A.6 of Annex A describe the detailed calculation including the pressure and temperature effects on the transducer ports as well as on the meter body. The detailed calculation process also allows the effects that individual parameters have on overall flow error to be assessed. Section A.8 of Annex A provides a worked example and observations on the method.

The detailed calculation contains estimates of extremes and allows the flow error to be described in either of the following equivalent forms:

$$Q_1/Q_0 = x.xxxx \pm x.xxxx \quad (12)$$
$$\Delta Q/Q = x.xx\ \% \pm x.xx\ \% \quad (13)$$

Stating the final flow correction factor, Q_1/Q_0, to 4 decimal places and flow error, $\Delta Q/Q$, to 2 decimal places is representative of the general level of accuracy of the calculation method. Since there will always be some uncertainty as to the actual end-loading conditions on the meter, the flow estimates will never be more precise than the tolerance values given in equations (12) and (13).

3 ADDITIONAL COMMENT

3.1 Use To Support or Check FE Models

Where the meter body is such that the body shape is not a simple cylinder, flanges take up a significant proportion of the total body length or ports are not simple tubes, an FE model will provide a more accurate estimate of the body and port dimensions and consequent flow error obtained from equation (2) than given by the calculations described in this paper.

As a means of checking the values from the FE model, the results for D, X, L and port lengths can be compared against those obtained from equations (A.5) through (A.8) including any flange or body style correction effect as in Sections A.3 where relevant and port effects as in Section A.5. If the meter body wall is irregular or non-cylindrical (for example as might be the case for a cast body) then, for the purposes of checking against the FE model, the direct calculations can be run for two scenarios: one where the outside radius, a, used in equation (A.5) through (A.8) is taken as the point where the wall is thinnest and then for the case where the outside radius is based on the point where the wall is thickest.

Since FE analysis deals with absolute change in physical dimensions, closer agreement with the direct calculation method of Sections A.2 through A.6 in Annex A will be obtained for actual meter dimensions D, X and L at given conditions if the calculation and FE runs are carried out as a three-stage process as described in Annex A, Section A.1

Care however needs to be taken in choice of the boundary conditions used for the FE model since these are often not easy to estimate for a given installation. It is recommended that models are run for a variety of different boundary conditions so that the sensitivity to the boundary conditions can be assessed. This is essentially similar to including the No-Ends and Capped-Ends cases in the direct calculation approach of Annex A, Sections A.2 through A.6.

3.2 Intentional Use of Thin-Wall Equations Beyond Their Normal Limits

In the fields of stress analysis and pressure vessel design, it is generally accepted that thin wall theory is only applied where d/R < 0.1. The reasons for this are that as d/R increases the difference with the more exact thick-shell theory grows unacceptably large at least as far as prediction of wall stress levels are concerned. Fig.5 shows the effect on ΔR/R of the various approaches (as given in equations A.5, A.7, A.9 and A.11) for different d/R ratios.

Fig.5 shows that d/R ratios higher than 0.1 give differences in ΔR/R of more than 10% compared to the thick-shell theory for the same end loading conditions. For example, if d/R = 0.247 the differences are 21% to 27% depending on which loading configuration is applied.

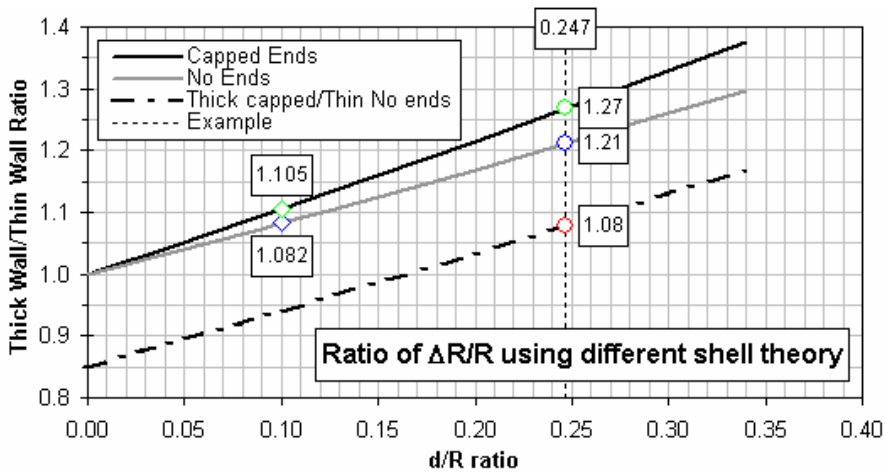

Fig. 5 - Comparison of thick-shell with thin-shell theory for different d/R ratios

If one mixes the loading cases and uses the thin-wall No-Ends equations for a thick-wall Capped-Ends situation, then one overestimates $\Delta R/R$ for d/R ratios < 0.16 and underestimates for d/R ratios > 0.16. For example, if d/R = 0.247, the underestimate in $\Delta R/R$ is 8%

Fig.5 shows that the thin-wall equations predict lower values of $\Delta R/R$ than the more exact thick-shell theory for the same load conditions. This produces a similar effect to using thick-shell theory plus an end load correction and body style correction as in Annex A, Section A.5 although how similar will depend on the actual geometry, flange-proximity and end loading conditions for a given meter.

In combination with FE modelling it may, for these reasons be found that a simple thin-shell theory gives adequate agreement to FE results for a given meter geometry and can subsequently be used as a valid means of estimating metering error at other conditions. It should be cautioned however that this will only apply to the specific meter on which the FE analysis was shown to give agreement and should not be taken as a general rule that can be applied to all meters.

4 CONCLUSION

A direct calculation method has been presented that allows estimates to be made of flow correction for geometry related pressure and temperature effects. The method provides traceability to its calculations and is applicable to a wide range of types and size of USFM and should provide a rapid means of estimating these types of flow error either for liquids or gas. The method also provides traceability to some of the correction equations used in earlier Standards and industry practice documents. The method can be used as a tool on its own or if the meter body is complex in shape, to supplement or check the results of FE analysis.

5 NOTATION

A	Meter bore section area (m^2)
a	Outside radius of meter body (m)
b	Chord diameter ratio
D	Inner diameter of body (m)
D_P	Outer diameter of body (m)
d	Meter body wall thickness (m)
$d_{p,o}$	Outer diameter of port tube (m)
$d_{p,i}$	Inner diameter of port tube (m)
E	Young's modulus of body (N/m^2)
E_p	Young's modulus of port (N/m^2)
E_t	Young's modulus of transd. (N/m^2)
K_E	End load correction factor
K_S	Body style correction factor
L	Path length (m)
L_p	Port length excluding flanges (m)
L_t	Transducer length (m)
N	Number of bounces on given path
P	Pressure (N/m^2)
Q	Volume flowrate (m^3/s)
R	Inside radius of meter body (m)
T	Temperature (°C)
t	time (s)
v	Flow velocity (m/s)
W	Mid path ratio
W_a	Average path distance ratio
X	Axial separation of ports (m)
Y	Left path distance ratio
Z	Right path distance ratio
α	Expansion coefficient (1/°C)
α_p	Port expansion coef. (1/°C)
α_t	transducer expansion coef. (1/°C)
Δ	Change in parameter
ϕ	Path angle (°)
σ	Poison's ratio of body material

Subscripts:

0, 1, 2, x …	parameter at conditions 0, 1, 2, x etc...

6 REFERENCES

[1] Lunde, P., Frøysa, K.-E., "Ormen Lange ultrasonic gas flow meters - A study for establishment of corrections for pressure and temperature effects", CMR-06-A10048-RA-01, Bergen (Norway) - 12/03/2007.

[2] Lunde, P., Frøysa, K-E, Folkestad, T., "Pressure and temperature effects for Ormen Lange ultrasonic gas flow meters", 25th International North Sea Flow Measurement Workshop, Norway, 16 - 19 October 2007.

[3] BS 7965:2000, "The selection, installation, operation and calibration of diagonal path transit time ultrasonic flowmeters for industrial gas applications. (being revised; possible issue late 2008 or early 2009)

[4] AGA Report No.9, "Measurement of Gas by Multipath Ultrasonic Meters". 2nd Edition (2007). (Recommended Practice)

[5] API MPMS 5.8 (2005). "MPMS Chapter 5 – Metering, Section 8 – Measurement of Liquid Hydrocarbons by Ultrasonic Flow Meters Using Transit Time Technology".

[6] Freund, W., Zanker, K., Goodson, D., Hall, J.E., Jamieson, A.W., "Operation of ultrasonic flow meters at conditions different than their calibration". NSFMW 2002, Scotland.

[7] "Review of report: Ormen Lange ultrasonic gas flow meters - A study for establishment of corrections for pressure and temperature effects", TUV NEL - report 2007/290 for Norwegian Petroleum Directorate, December 2007.

[8] Roark: Young, W.C., Budynas, R.G., "Roark's formulas for stress and strain", 7th Edition. McGraw-Hill. New York. 2001

[9] ISO/CD 17089-1 "Measurement of fluid flow in closed conduits - Ultrasonic Meters for gas -- Part 1: Meters for custody transfer and allocation measurements". July 2008.

[10] BS 8452:2005, "Use of clamp-on (externally mounted) transit time metering techniques for liquid applications – guide". (being revised)

ANNEX A

Detailed Calculation of Geometry-Related Temperature and Pressure Corrections

A.1 Single-Stage Calculation or Three-Stage Calculation ?

Since the physical dimensions of the meter will most likely have been measured under static calibration conditions, the flow calibration carried out under dynamic calibration conditions and the meter used under field conditions, the calculation of the flow correction required between dynamic calibration and field conditions can be carried out as a three-stage process [1].

1) Calculate the flow correction from static calibration to dynamic calibration using:

$$\frac{Q_1}{Q_0} = \left(\frac{D_1}{D_0}\right)^2 \left(\frac{L_1}{L_0}\right)^2 \left(\frac{X_0}{X_1}\right) \qquad \text{(A.1)}$$

2) Calculate the flow correction from static calibration to field conditions using:

$$\frac{Q_2}{Q_0} = \left(\frac{D_2}{D_0}\right)^2 \left(\frac{L_2}{L_0}\right)^2 \left(\frac{X_0}{X_2}\right) \qquad \text{(A.2)}$$

3) Calculate the difference between dynamic calibration and field conditions using:

$$\frac{Q_2}{Q_1} = \frac{Q_2}{Q_0} \cdot \frac{Q_0}{Q_1} = \left(\frac{D_2}{D_1}\right)^2 \left(\frac{L_2}{L_1}\right)^2 \left(\frac{X_1}{X_2}\right) \qquad \text{(A.3)}$$

Or:

$$\frac{\Delta Q_{2,1}}{Q} = \frac{Q_2}{Q_1} - 1 \qquad \text{(A.4)}$$

This three-stage approach is useful if a check on the actual physical dimensions at intermediate stages within the calculations is required as, for example, might be the case if specific dimensions are to be compared against FE modelling. However, as can be seen in equation (A.3), the calculation can be carried out in a direct single-stage (i.e. from dynamic calibration to field operation conditions) rather than the more lengthy three-stage process since the actual flow correction between these two conditions involves the relative change in dimensions, not the absolute values.

A.2 Direct Calculation – Body Pressure Expansion

The effect of a pressure change is to alter the diameter and length of the meter body but the actual change in dimensions depends on a number of factors including:

- The thickness/inner radius ratio of the meter walls {i.e. the ratio d/R = (a-R)/R = (a/R)-1}
- The way the meter is supported and attached to or constrained by adjacent pipework
- The rigidity of the adjacent pipework
- Any axial loading
- The general geometry of the meter body and whether it has flanges
- The slenderness ratio of the meter (i.e. the overall body length/body diameter)

The way end constraining loads and end pressure loads are applied to the meter will vary from one installation to another. We use two standard simple load conditions to provide the extremes in load situation the body will be exposed to; we will refer to these as the “No-Ends” case and the “Capped-Ends” case. In practice the particular way a meter is installed should result in conditions somewhere between these two extremes.

For a thick-wall body (i.e. d/R>0.1) with only radial internal pressure but no end loads (the No-Ends condition) as show in Fig.A.1, for positions well away from ends Roark [8] gives:

$$\frac{\Delta R}{R} = \frac{\Delta P}{E}\left(\frac{a^2 + R^2}{a^2 - R^2} + \sigma\right) \tag{A.5}$$

$$\frac{\Delta X}{X} = \frac{-\Delta P.\sigma}{E}\left(\frac{2.R^2}{a^2 - R^2}\right) \tag{A.6}$$

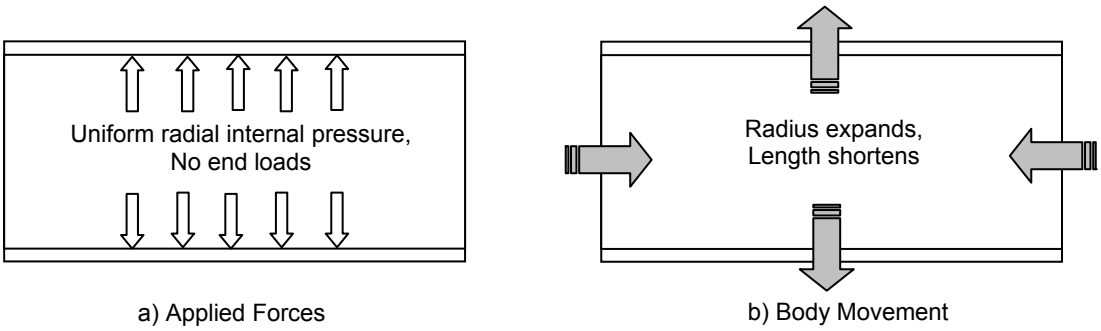

Fig.A.1 - Applied forces and resulting body change for No-Ends

And for radial internal pressure plus pressure end load (the Capped-Ends condition) as shown in Fig.A.2, for positions well away from ends, Roark gives:

$$\frac{\Delta R}{R} = \frac{\Delta P}{E}\left(\frac{a^2(1+\sigma) + R^2(1-2.\sigma)}{a^2 - R^2}\right) \tag{A.7}$$

$$\frac{\Delta X}{X} = \frac{\Delta P}{E}\left(\frac{R^2(1-2.\sigma)}{a^2 - R^2}\right) \tag{A.8}$$

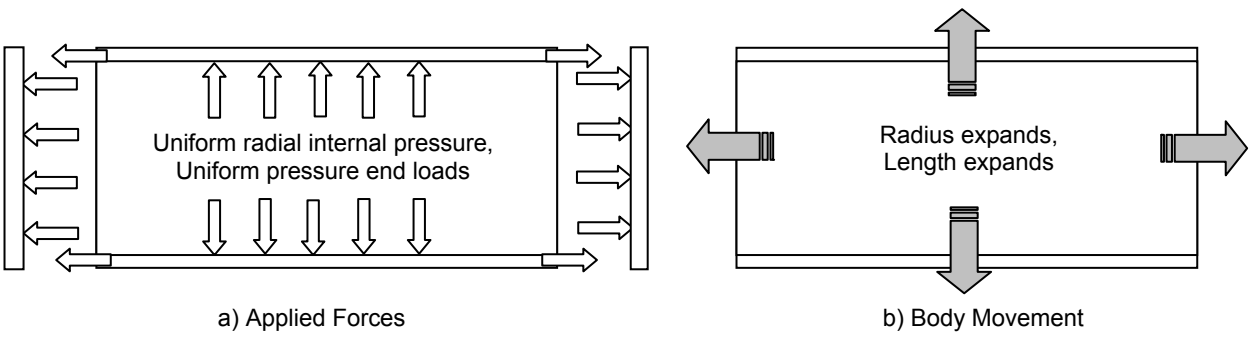

Fig A.2 – Applied forces and resulting body change for Capped-Ends

For a thin-wall body (d/R<=0.1) for only radial internal pressure (No-Ends) and positions well away from ends, Roark gives simpler equations as:

$$\frac{\Delta R}{R} = \frac{\Delta P.R}{E.d} \tag{A.9}$$

$$\frac{\Delta X}{X} = \frac{-\Delta P.R.\sigma}{E.d} \tag{A.10}$$

And, for Capped-Ends:

$$\frac{\Delta R}{R} = \frac{\Delta P.R}{E.d}\left(1 - \frac{\sigma}{2}\right) = 0.85\frac{\Delta P.R}{E.d} \quad for\,\sigma = 0.3 \tag{A.11}$$

$$\frac{\Delta X}{X} = \frac{\Delta P.R}{E.d}\left(0.5 - \sigma\right) \qquad \text{(A.12)}$$

For all meter types, the meter ends are assumed to be unconstrained and free to move axially.

It should be noted that the thick-wall equations (A.5 through A.8) are the more exact since they also cover the simpler case of thin-wall pipe (equations A.9 through A.12). Consequently, for all meter body types, thick-shell theory is the preferred approach since this is more general than thin-shell theory. These equations are often the fundamental basis, but not specified explicitly, of correction factors quoted in earlier Standards or industry documents, e.g. [4], [5].

Essentially the choice of whether to use thin or thick-shell theory is based on the ratio d/R. In practice this effectively means that the choice of equations is related to the pressure rating of the body since meters for high pressure systems will have thicker walls than meters for low pressure systems. Generally, meter spools up to ANSI 900 designed in accordance with ASME rules and using one of the most common steel types (A333 steel), fall in the thin-wall range. This is also true for many of the ANSI 1500 meters made from high tensile steel.

Thin-wall equations are generally not used where d/R>0.1 but can be used as described in Section 3.2 for thick wall vessels in combination with FE modelling (Section 3.1) if the limitations are understood as an alternative to applying a style correction as in Section A.3.

A.3 Direct Calculation – Correction for Body Style Effect or Proximity to Flanges

If portions of the ultrasonic path are closer than one outside pipe diameter, D_P, to flanges or the body is of irregular shape, the radial expansion will be less than that indicated by equations A.5 and A.7 (or A.9 and A.11 for a thin-walled body) due to local stiffening effects. To compensate for this local stiffening effect a “style correction factor”, K_s, is introduced.

K_s will always be less than or equal to 1 and the value used for specific body types is:

- For a welded-in body with no flanges within $1.D_P$ of the ultrasonic transducer locations, $K_s = 1$, i.e. the meter body behaves as a simple pipe.
- For a flanged meter body (for example, consisting of two flanges welded to a pipe), or welded-in design where neighboring flanges are within $1.D_P$ of the transducer positions, the value of K_s is calculated as follows:

It is assumed that the diametral expansion varies linearly from zero at the flange to the value given by equations (A.5) and (A.7) (or A.9 and A.11 for thin-wall) at one external diameter or greater from the flange. It is also assumed for simplicity that the flange correction only affects the radial expansion of the body, not the linear expansion in the vicinity of the ultrasonic paths.

The transducer port positions are described as shown in Figure A.3 in terms of the body outer diameter D_P.

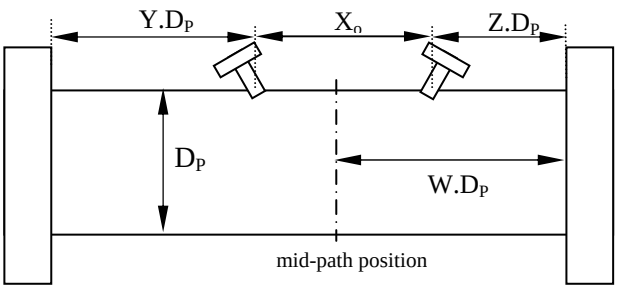

Fig. A.3 - Transducer port proximity to flanges

Since the ultrasonic path covers a range in axial distance from a flange, the average path distance, $W_a.D_P$, is calculated from three positions on a given path; W, at the mid-path position and Y and Z, at the actual transducer locations. W, Y and Z are distances to the nearest flange from their respective positions.

If any of the values of W, Y or Z are greater than 1, then the value used for that parameter in the calculation is limited to a value of 1.
Where the meter's transducers are clearly all closer to one flange than the other, the alternative arrangement as in Figure A.4 is used.

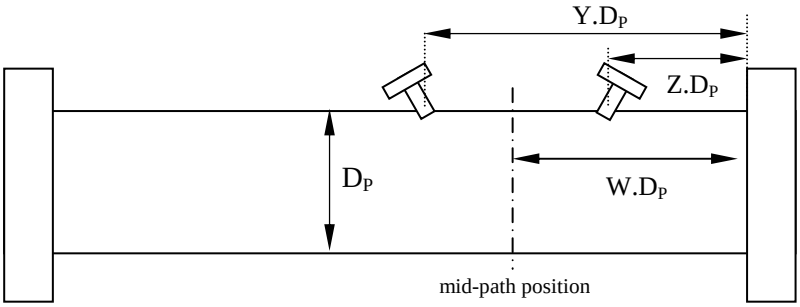

Fig. A.4 - Transducer port proximity to flanges – long meter with offset ports

The average path distance, W_a, from a flange is calculated from:

$$W_a.D_P = \left\{\frac{W+Y+Z}{3}\right\}.D_P \qquad \text{(A.13)}$$

The style correction, K_s, is obtained using:

$$K_S = \frac{W_a}{1} \qquad \text{(A.14)}$$

A stiffening effect will also occur near any part of the body which has features such as branches or welds. These generally create less of an effect than proximity to flanges since they typically occupy only a small portion of the body circumference.

A.4 Direct Calculation – Combined Pressure Correction Effect

The radial expansion of the body, including flange correction, is calculated from:

$$D_1 = D_0\left(1+K_s.\frac{\Delta D}{D_0}\right) = D_0\left(1+K_s.\frac{\Delta R}{R}\right) \Rightarrow \frac{D_1}{D_0} = 1+K_s.\frac{\Delta R}{R} \qquad \text{(A.15)}$$

The axial expansion of the body is calculated from:

$$X_1 = X_0\left(1+\frac{\Delta X}{X}\right) \Rightarrow \frac{X_1}{X_0} = 1+\frac{\Delta X}{X} \qquad \text{(A.16)}$$

Note as previously mentioned, the style correction effect is only applied for the radial expansion of the body as in equation (A.15)

The path length is calculated from:

$$L_0^{\ 2} = (N+1)^2 \cdot b^2.D_0^{\ 2} + X_0^{\ 2} \qquad \text{(A.17)}$$

$$L_1^{\ 2} = (N+1)^2 \cdot b^2.D_1^{\ 2} + X_1^{\ 2} \qquad \text{(A.18)}$$

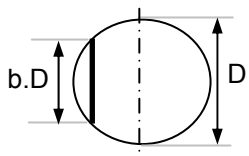

Fig. A.5 Chord Ratio

Note that, N = 0 for a single traverse path and from Fig A.5, b = 1 for a diametral path.

Hence, for a given meter with a known wall thickness, d, and initial geometry X_0, D_0 and L_0 at reference conditions, the revised dimensions X_1, D_1 and L_1 can be calculated for the pressure difference using equations (A.15) through (A.18).

The flow correction factor is then calculated using:

$$\left(\frac{Q_1}{Q_0}\right)_{bodypressure} = \left(\frac{D_1}{D_0}\right)^2 \left(\frac{L_1}{L_0}\right)^2 \left(\frac{X_0}{X_1}\right) \qquad \text{(A.19)}$$

The error correction obtained from equation (A.19) for the No-Ends case and for the Capped-Ends cases are calculated as described in Section A.2, to give a range of correction factor. This range should generally be small and the process sufficient to provide an indication of the flow correction required.

A.5 Direct Calculation - Expansion Effects in the Transducer Ports

In addition to the effects that pressure and temperature changes have on the meter body they also alter the lengths of the transducer ports. This actually moves the position of the transducer face and hence affects the acoustic path-length. Although this effect is generally small, a simple procedure is included here to allow the effects on the ports to be estimated. Fig. A.6 shows the port geometry dimensions used for this assessment.

Temperature and pressure corrections are treated separately and for both, the only effect that is considered here is the path length change.

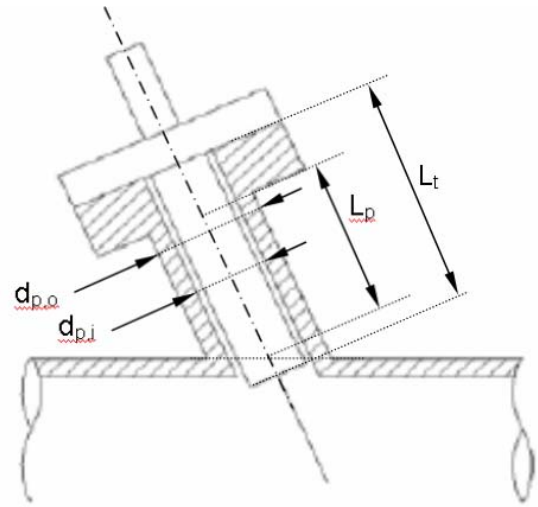

Fig. A.6 - Port dimensions

- **Temperature Correction -** Due to the way the transducer is secured into the port, it is generally held at the end of the port. The consequence of this is that any expansion of the port itself will occur in the opposite direction to the expansion of the transducer; hence the expansions will to some extent cancel depending on the relative thermal expansion coefficient of the port material, α_p, and the transducer material, α_t. The change in transducer face position, ΔL_t, due to temperature is given by:

$$\Delta L_t = L_t\left(\alpha_p.\Delta T - \alpha_t.\Delta T\right) = L_t.\left(\alpha_p - \alpha_t\right).\Delta T \qquad \text{(A.20)}$$

This is the change in face position in each port so the effect on a given ultrasonic path will be $2*\Delta L_t$. Assuming there is no diameter change or axial change equation (2), solely for the port expansion, simplifies to:

$$\left(\frac{Q_1}{Q_0}\right)_{porttemperature} = \left(\frac{L_1}{L_0}\right)^2 = \left[\frac{L_0 + 2.\Delta L_t}{L_0}\right]^2 = \left[1 + \frac{2.L_t.\left(\alpha_p - \alpha_t\right).\Delta T}{L_0}\right]^2 \qquad \text{(A.21)}$$

For small values this gives:

$$\left(\frac{Q_1}{Q_0}\right)_{porttemperature} = \left[1 + \frac{4.L_t.(\alpha_p - \alpha_t).\Delta T}{L_0}\right] \quad \text{(A.22)}$$

or alternatively:

$$\left(\frac{\Delta Q}{Q}\right)_{porttemperature} = 4.(\alpha_p - \alpha_t).\frac{L_t}{L_0}.\Delta T \quad \text{(A.23)}$$

- **Pressure Correction** – The pressure effect on the port and the transducer act in the same direction; the port is stretched whilst the transducer is compressed. For this simple approach the port and transducer are assumed to act as simple linear elastic materials. The linear strain in the port walls is given by:

$$\Delta L_p = L_t.\frac{\Delta P}{E_t} + L_p.\frac{\Delta P}{E_p}.\left(\frac{d_{pi}^{\ 2}}{d_{po}^{\ 2} - d_{pi}^{\ 2}}\right) = \Delta P.\left[\frac{L_t}{E_t} + \frac{L_p}{E_p}.\left(\frac{d_{pi}^{\ 2}}{d_{po}^{\ 2} - d_{pi}^{\ 2}}\right)\right] \quad \text{(A.24)}$$

This is the change in face position in each port. Assuming there is no diameter change or axial change equation (2), solely for the port pressure expansion, simplifies to:

$$\left(\frac{Q_1}{Q_0}\right)_{portpressure} = \left(\frac{L_1}{L_0}\right)^2 = \left[\frac{L_0 + 2.\Delta L_p}{L_0}\right]^2 = \left[1 + \frac{2.\Delta L_p}{L_0}\right]^2 \quad \text{(A.25)}$$

this for small values gives:

$$\left(\frac{Q_1}{Q_0}\right)_{portpressure} = \left[1 + \frac{4.\Delta L_P}{L_0}\right] \quad \text{(A.26)}$$

or alternatively to:

$$\left(\frac{\Delta Q}{Q}\right)_{portpressure} = 4.\frac{\Delta L_p}{L_0} \quad \text{(A.27)}$$

- **Combined port correction** – This is calculated using:

$$\left(\frac{Q_1}{Q_0}\right)_{ports} = \left(\frac{Q_1}{Q_0}\right)_{portpressure} * \left(\frac{Q_1}{Q_0}\right)_{porttemperature} \quad \text{(A.28)}$$

A.6 Direct Calculation - Combined Flow Correction

The combined flow correction factor for a given set of pressure and temperature conditions is obtained from:

$$\frac{Q_x}{Q_0} = \left(\frac{Q_x}{Q_0}\right)_{bodypressure} * \left(\frac{Q_x}{Q_0}\right)_{bodytemperature} * \left(\frac{Q_x}{Q_0}\right)_{ports} \quad \text{(A.29)}$$

which can be expressed as the flow error:

$$\frac{\Delta Q_{x,0}}{Q} = \frac{Q_X}{Q_0} - 1 \quad \text{(A.30)}$$

For small values of correction this simplifies to:

$$\frac{\Delta Q_{x,0}}{Q} = \left(\frac{\Delta Q_x}{Q_0}\right)_{bodypressure} + \left(\frac{\Delta Q_x}{Q_0}\right)_{bodytemperature} + \left(\frac{\Delta Q_x}{Q_0}\right)_{ports} \quad \text{(A.31)}$$

Two values for the combined flow correction are obtained; one using the No-Ends pressure correction and one using the Capped-Ends pressure correction described in Section A.2. This allows the flow error to be expressed in either of the equivalent forms as in equations (12) and (13), i.e. Q_x/Q_0 = x.xxxx ± x.xxxx or $\Delta Q/Q$ = x.xx % ± x.xx %

A.7 Calculation of an Initial Estimate for the Maximum Body Pressure Effect

To provide the initial estimate of the body pressure effects used in Section 2.3.1, for simplicity the axial change in X and any flange proximity or body style effect, K_S, are neglected; i.e. K_S=1. Using equations (A.15), (A.17) and (A.18), equation (A.19) reduces to:

$$\left(\frac{Q_1}{Q_0}\right)_{bodypressure,estimate} = \left(\frac{D_1}{D_0}\right)^2\left(\frac{L_1}{L_0}\right)^2 = \left(\frac{D_1}{D_0}\right)^2\left(\frac{D_1}{D_0}\right)^2 = \left(\frac{D_1}{D_0}\right)^4 = \left(1+\frac{\Delta R}{R}\right)^4 \quad \text{(A.32)}$$

For small values of $\Delta R/R$ this reduces further, by ignoring higher order terms, to:

$$\left(\frac{Q_1}{Q_0}\right)_{bodypressure,estimate} = \left(1+\frac{\Delta R}{R}\right)^4 \approx 1 + 4\cdot\frac{\Delta R}{R} \quad \text{(A.33)}$$

or in terms of $\Delta Q/Q$ gives:

$$\left(\frac{\Delta Q}{Q}\right)_{bodypressure,estimate} = \frac{Q_1}{Q_0} - 1 = 4\cdot\frac{\Delta R}{R} \quad \text{(A.34)}$$

The No-Ends, Thick-wall equation (A.5) is used for $\Delta R/R$ to give a worst-case estimate since it produces the largest change in $\Delta R/R$ for a given applied ΔP. Hence the maximum expected $\Delta Q/Q$ due to body pressure change effects is given by:

$$\left(\frac{\Delta Q}{Q}\right)_{bodypressure,\max imum} = 4\cdot\frac{\Delta R}{R} = 4\cdot\left(\frac{a^2+R^2}{a^2-R^2}+\sigma\right)\cdot\frac{\Delta P}{E} \quad \text{(A.35)}$$

A.8 Worked Example - a Flanged-Body Spool Meter

A.8.1 Meter details

Note, only details marked* are needed for the initial estimate

Body Inner radius*	=	183.25	= R_o	(mm)
Body outer radius*	=	228.6	= a	(mm)
Wall thickness*	=	45.35	= d	(mm)
Transducer Port length	=	230	= L_p	(mm)
Port outer diameter	=	50	= $d_{p,o}$	(mm)
Port inner diameter	=	32	= $d_{p,i}$	(mm)
Proximity of port to left hand flange*	=	366		(mm)
Proximity of port to right hand flange*	=	686		(mm)
Single bounce path	=	1	= N	--
Chord diameter ratio	=	1 (i.e. diametral path)	= b	--

Path Angle	=	70	= ϕ	(°)
Path Length	=	780.117	= L_o	(mm)
Transducer Separation	=	267.007	= X_o	(mm)
Body Material Young's Modulus* (N/m^2)	=	2.00e+11	=	E
Poison's ratio*	=	0.3	= $\tilde{\sigma}$	
Thermal Expansion Coefficient*	=	1.26e-05	= α	(1/°C)
Port length excluding flange	=	220	= Lp	(mm)
Transducer diameter	=	32	= d_t	(mm)
Transducer length	=	230	= L_t	(mm)
Transducer Thermal expansion (estimated)	=	1.5e-05	= α_t	(1/°C)
Transducer Young's Modulus (estimated)	=	1.9e+11	= E_t	(N/m^2)
Static-calibration conditions	=	0 bar gauge, 20 °C		
Dynamic-calibration conditions*	=	63 bar gauge, 7 °C		
Field operation conditions*	=	230 bar gauge, 40 °C		
Meter Class	=	1 (Custody Transfer)		

These are first used to calculate some common basic parameters:

Wall thickness ratio, d/R		=	0.2475	implies "thick-wall"	
Meter external diameter		=	2*228.6	= 457.2	= D_P
Flange proximity	– closest	=	366/457.2	= 0.8 D_P	=>Z=0.8
	- further	=	(366+267)/457.2 = 1.38 D_P		=>Y =1
	- mid-path	=	(366+0.5*267)/457.2 = 1.09 D_P		=>W =1
Body style correction factor		=	(W+Y+Z)/3 = 2.8/3		= 0.93 =K_S

A.8.2 Initial flow error estimate

Using the simple estimates from Figures 2 and 3 of Section 2.2 and 2.3.1, the expected $\Delta Q/Q$ flow errors from dynamic-calibration to field operating conditions are +0.13% for ΔT=+33°C, and +0.16%*0.93 = + 0.15% for ΔP=+167 bar.

From Fig.4, for d/R = 0.247, the end correction K_E = 0.89 and this gives a lower estimate of 0.13% (i.e. 0.89 *0.15%) for the pressure term.

This gives a combined initial estimate for the flow error of **+0.26%** to **+0.28%** (or 0.27% ± 0.01%) which is, referring to Table 2, significant for a Class 1 meter and therefore a detailed calculation is needed.

A.8.3 Common elements to a detailed calculation

Common elements to the detailed calculation for any ΔP and E ratio are:

Port pressure length change from equation (A.24)

$$\Delta L_p = \Delta P\left[\frac{230}{1.9e+11} + \frac{220}{2e+11}\left(\frac{32^2}{50^2 - 32^2}\right)\right] = 1.97367 * 10^{-9} * \Delta P$$

Equations (A.5) through (A.8) give, for No-Ends:

$$\frac{\Delta R}{R} = \left(\frac{228.6^2 + 183.25^2}{228.6^2 - 183.25^2} + 0.3\right)\frac{\Delta P}{E} = 4.89585\frac{\Delta P}{E}$$

$$\frac{\Delta X}{X} = -0.3 * \left(\frac{2 * 183.25^2}{228.6^2 - 183.25^2} \right) \frac{\Delta P}{E} = -1.07876 \frac{\Delta P}{E}$$

and for Capped-Ends:

$$\frac{\Delta R}{R} = \left(\frac{1.3 * 228.6^2 + 0.4 * 183.25^2}{228.6^2 - 183.25^2} \right) \frac{\Delta P}{E} = 4.35647 \frac{\Delta P}{E}$$

$$\frac{\Delta X}{X} = \left(\frac{0.4 * 183.25^2}{228.6^2 - 183.25^2} \right) \frac{\Delta P}{E} = 0.71917 \frac{\Delta P}{E}$$

Note: the ratio between Capped-Ends and No-Ends, i.e. K_E, for $\Delta R/R$ is = 4.35647/4.89585 = 0.89 as would be obtained from Fig.4.

For interest, the thin-walled pipe equations (A.9) through (A.12) would give, for No-Ends:

$$\frac{\Delta R}{R} = \frac{183.25}{45.35} \frac{\Delta P}{E} = 4.04079 \frac{\Delta P}{E}$$

$$\frac{\Delta X}{X} = -0.3 * \frac{183.25}{45.35} \frac{\Delta P}{E} = -1.21224 \frac{\Delta P}{E}$$

and for Capped-Ends:

$$\frac{\Delta R}{R} = 0.85 * \frac{183.25}{45.35} \frac{\Delta P}{E} = 3.43467 \frac{\Delta P}{E}$$

$$\frac{\Delta X}{X} = 0.2 * \frac{183.25}{45.35} \frac{\Delta P}{E} = 0.80816 \frac{\Delta P}{E}$$

The thin-wall results are only shown here for example since the actual d/R ratio being used is 0.247. Note however that the ratio of thick-wall to thin-wall $\Delta R/R$ = 4.89585/4.04079 = 1.21 for d/R = 0.247 for No-Ends and $\Delta R/R$ = 4.35647/3.43467 = 1.27 for Capped-Ends. These were the values used in the example in Fig.5.

A.8.4 Single-stage detailed calculation

For the example, the temperature and pressure difference between dynamic-calibration and field operation is: ΔT = 40 – 7 = +33 °C, ΔP = 230 – 63 = +167 bar. This gives:

$\Delta P/E$	$= 167*10^5/2*10^{11}$	$= 83.5 *10^{-6}$
ΔL_p	$= 167*10^5*1.97367*10^{-9}$	= 0.03295

1) Body temperature effect from equation (6):

Q_1/Q_0 $=1+3*1.26*10^{-5}*(33.0)$ **= 1.001247**

2) Body pressure effect from equation (A.5) through (A.8) and equation (A.35):

No-Ends:	$\Delta R/R$	$= 4.89585*83.5 *10^{-6}$	$= 4.08803 * 10^{-4}$
	$\Delta X/X$	$= -1.07876*83.5 *10^{-6}$	$= -0.90076 * 10^{-4}$
Initial body pressure estimate = 4. $\Delta R/R$			**= 0.164%**
Capped-Ends:	$\Delta R/R$	$= 4.35647*83.5 *10^{-6}$	$= 3.63766 * 10^{-4}$
	$\Delta X/X$	$= 0.71917*83.5 *10^{-6}$	$= 0.60051 * 10^{-4}$

Combined body pressure effect from equations (A.15) through (A.19) with K_S=0.93:

No-Ends:	D_1/D_0	= $(1+0.93*4.08803*10^{-4})$	= 1.000380
	D_1	= 1.000380*366.5	= 366.6393
	X_1/X_0	= $(1-0.90076*10^{-4})$	= 0.999910
	X_1	= 0.999910*267.007	= 266.9830
	L_1	= $\{(2)^2*1*366.6393^2+266.9830^2\}^{0.5}$	= 780.3701
	L_1/L_0	= 780.3701/780.117	= 1.000324
	Q_1/Q_0	= $1.000380^2*1.000324^2/0.999910$	**= 1.001499**
Capped-Ends:	D_1/D_0	= $(1+0.93*3.63766*10^{-4})$	=1.000338
	D_1	= 1.000338*366.5	= 366.6239
	X_1/X_0	= $(1+0.60051*10^{-4})$	= 1.0000601
	X_1	= 1.0000601*267.007	= 267.02304
	L_1	= $(4*1*366.6239^2+267.02304^2)^{0.5}$	= 780.3548
	L_1/L_0	= 780.3548/780.117	= 1.000305
	Q_1/Q_0	= $1.000338^2*1.000305^2/1.0000601$	**= 1.001226**

3) Port effects from equations (A.23), (A.27) and (A.28):

Temperature	Q_1/Q_0	= $\{1+4*230*(1.25-1.5)*10^{-5}*(33)/780.117\}$	= 0.999903
Pressure	Q_1/Q_0	= (1+4*0.03295/780.117)	= 1.000169
Combined	Q_1/Q_0	= 0.999903*1.000169	**= 1.000072**

4) Overall combined flow correction from equation (A.29):

No-Ends:	Q_1/Q_0	= 1.001247*1.001499*1.000072	= 1.002820
Capped-Ends:	Q_1/Q_0	= 1.001247*1.001226*1.000072	= 1.002547
	Q_1/Q_0		**= 1.002684±0.000136**
			= 1.0027 ± 0.0001

In terms of $\Delta Q/Q$ from equation (A.30) this is:

$\Delta Q_{1,0}/Q_0$ **= +0.2684 % ± 0.0136 %**
= +0.27 % ± 0.01%

A.8.5 Three-stage detailed calculation

For the sake of brevity, only the key outcomes of a worked example of a three-stage calculation are included here. The three-stage calculation involves using the common elements from Section A.8.3 (with K_S=0.93 and K_E=0.89) and a comparison of the difference between a repeat of the calculations of Section A.8.4 but for the two conditions for the temperature and pressure difference namely:

Case 1) - Static calibration to dynamic calibration, i.e. ΔT = 7-20 = -13 °C, ΔP = 63 bar.
Case 2) - Static calibration to field operation, i.e. ΔT = 40 –20 = +20 °C, ΔP = 230 bar.

Table A.1 shows the outcome of the calculations.

Table A.1 – Key outcomes of a Three-Stage calculation

Parameter	**Q_1/Q_0 Case 1)**	**Q_2/Q_0 Case 2)**	**Case 1) to Case 2)**
Initial body pressure estimate	$\Delta Q/Q$ = +0.062%	$\Delta Q/Q$ = +0.23%	---
Body Temperature	0.999509	1.000756	1.001248
Body Pressure No-Ends	1.000557	1.002070	1.001512

Capped-Ends	1.000463	1.001690	1.001226
Ports (ΔP & ΔT effects)	1.000102	1.000170	1.000067
Combined Correction Factor % Flow Error ΔQ/Q	1.00012±0.00005 +0.012%±0.005%	1.00281±0.00019 +0.281%±0.019 %	1.00269±0.00014 +0.269%±0.014%

A.9 Observations on the Example Calculation

Note that, for the sake of calculation accuracy, individual values during the calculations have generally been quoted to six significant figures but it should be realised this does not reflect the implied accuracy of the prediction method. It is felt that as stated in Section 2.6, the final overall flow correction factor, Q_2/Q_1, should be quoted to 4 decimal places and ΔQ/Q value to 2 decimal places.

It can be observed that in terms of final flow correction error between the dynamic-calibration conditions and operating conditions, the difference between the direct single-stage calculation of section A.8.4 and the more complex three-stage approach of section A.8.5 are negligible. As mentioned in Section A.1, the three-stage approach may however be more useful to compare intermediate results and specific dimensions with those from an FE model.

It is also noticeable that the initial flow error estimate made in section A.8.2 using the simple approach outlined in Section 2.3 is the same as the result of the more detailed calculation of sections A.8. This is most probably a feature of the example chosen since it would be expected there would be some minor difference.

The intermediate stages in the calculation are useful to gauge the relative sizes, and hence importance, of the flow correction effects due to:

- **Initial body pressure estimate** – The initial body pressure effect estimates were 0.062% and 0.23% for the two cases examined and these compare with values of 0.056% and 0.21% from the more detailed calculation. In both cases, as expected, the initial estimate is higher than the more detailed calculation.

- **Meter end loading conditions** – the variation in end loading only affects the change in body dimensions due to pressure effects. The use of the No-Ends condition and the Capped-Ends condition provides an indication of the sensitivity of the correction to the end loading conditions. In the two cases looked at, the variation between the No-Ends and Capped-Ends cases is only +0.05% to +0.06% for Case 1 and +0.17% to +0.21% in Case 2. This would indicate that the end-loading conditions are of secondary importance.

- **Body pressure effect – for the two cases considered, the body pressure was of** the order of +0.05% in Case 1 (63 bar) and +0.2% in Case 2 (230 bar). Of that, the area effect, due to $(D_1/D_0)^2$, was of the order of 0.027% and 0.09% respectively for the two cases; hence the area effect accounts for roughly half of the flow correction.

- **Body temperature effects** – for the two cases considered, the body temperature effects were -0.05% for Case 1 (-13°C) and +0.08% for Case 2 (+20°C). This would indicate that temperature effects are as important as pressure effects. Note that in Case 1, because the ΔT was negative, its effect partly cancelled the pressure effect whereas in Case 2, ΔT was positive and its effect added to the pressure effect.

- **Port effects** – Due to the way transducers are held into the port it is possible for the temperature effects to cancel (i.e. port extension is cancelled by transducer growth). The combined pressure and temperature effect in Case 1 was +0.01% and for Case 2 was +0.02%. This would indicate that transducer port effects are an order of magnitude smaller than either the temperature or pressure effects on the meter body itself.

- **Comparison against the results of an FE model** – The pressure and temperature conditions and meter dimensions used in the worked example have been based on a meter and conditions that have also been used in an FE model [1], [2]. Results from the FE model show flow errors of +0.003% to +0.006% for single-bounce diametral paths for Case 1 and combined flow error for the difference between Case 2 and Case 1 of +0.264% to +0.272%. These compare very favourably with the +0.0121% ± 0.0047% for Case 1 and +0.27% ± 0.01% for the combined Case 2-Case 1 calculated above in section A.8. Agreement is to within 0.01% on overall % flow error.

It is realised that these observations are made on the particular cases examined in this specific example. It can consequently be expected there will be some variation between the importance of different effects with different metering models and operating conditions. It is however expected that the relative importance of specific effects will still be consistent with the observations made from the example calculations.

North Sea FLOW Measurement Workshop

Paper 6.3

Installation Effects on the Easington Ultrasonic Fiscal Metering Station

Kjell-Eivind Frøysa
Christian Michelsen Research AS

Anders Hallanger
Christian Michelsen Research AS

Anfinn Paulsen
Gassco AS

TÜV SÜD

nel technology for life

Installation Effects on the Easington Ultrasonic Fiscal Metering Station

Kjell-Eivind Frøysa, Christian Michelsen Research AS
Anders Hallanger, Christian Michelsen Research AS
Anfinn Paulsen, Gassco AS

1 INTRODUCTION

The gas from Norway's Ormen Lange gas field is imported to UK at the Langeled Receiving Facilities (LRF) in Easington. This section of the terminal is operated by Centrica on behalf of Gassco. Eventually up to 25 % of the UK gas demand may be served from this pipeline alone. The fiscal metering station for the Ormen Lange gas consists of ultrasonic meters installed in four parallel meter pipes. The design has some deviations from the conventional design, i.e. no flow straightening devices and long upstream lengths (~55D) to the metering point. At the ultrasonic flow meters, asymmetric velocity profiles are observed. Because of the possibility of increased uncertainty in the measured gas amount due to these asymmetries, CMR and Gassco have carried out an investigation of the installation effects of the metering station at Easington.

In the present work, the results from this investigation are presented. A Computational Fluid Dynamics (CFD) model for the inlet header and the metering sections is established, and simulations are carried out covering a range of flow rates. To investigate the sensitivity of the meters to flow variations in header, different inlet flow velocity profiles including rotation are applied. Measurement configurations with all four metering sections in use and with one or two metering sections closed are covered. Comparisons show good agreement between the CFD analyses and the measurement. The calculated flow velocity fields are thereafter taken as input to a computer program where the ultrasonic flow meter is modelled. Here the average velocities along the sound paths are calculated as well as an accurate estimate of the average (reference) flow velocity. The integration algorithms used in the flow computer are applied to calculate the average velocity from the sound path velocities, and the results are compared with the reference velocities. Other parameters like swirl are also considered. In addition to the results at the meter locations, virtual meter installations upstream in the metering sections are also considered. In the bulk of the cases, the deviation from the flow calibration (simulated) for the four ultrasonic flow meters is in the range 0.05-0.25 %. For all cases except one, the deviations from reference at the meter installations are less than ± 0.3 %.

2 INSTALLATION GEOMETRY AND FLOW DATA

The metering station and the upstream piping are shown in Figure 1. It is there seen that the header is asymmetric (when considering the inlet relative to the four metering sections). This layout has been made in order to achieve easy access to all meters and associated instrumentation from two different platforms. The simulation geometry starts at the header inlet, position A in the figure, and ends in the manifold downstream of the 4 parallel metering sections, position B in the figure. Each of the metering sections can be closed by valves, position C in the figure.

The four parallel metering sections are each equipped with an FMC MPU1200 ultrasonic flow meter [1]. The calculations of the flow will be carried out from the inlet of the metering header, through all four metering runs and through the pipes and manifold downstream of the meters.

The inlet valve of each metering section is set to be totally open, and the unit is modeled as an empty pipe.

The inner diameter of the header pipe is 0.987 m. In the metering section, the inner diameter is 0.560 m (~24”). At the manifold downstream the metering sections, the inner diameter is set to 0.987 m.

The bend between the header and each of the parallel metering pipes has a bend radius of 1.71 m. The bend radius in the header pipe S-bend is set to 2.75 m.

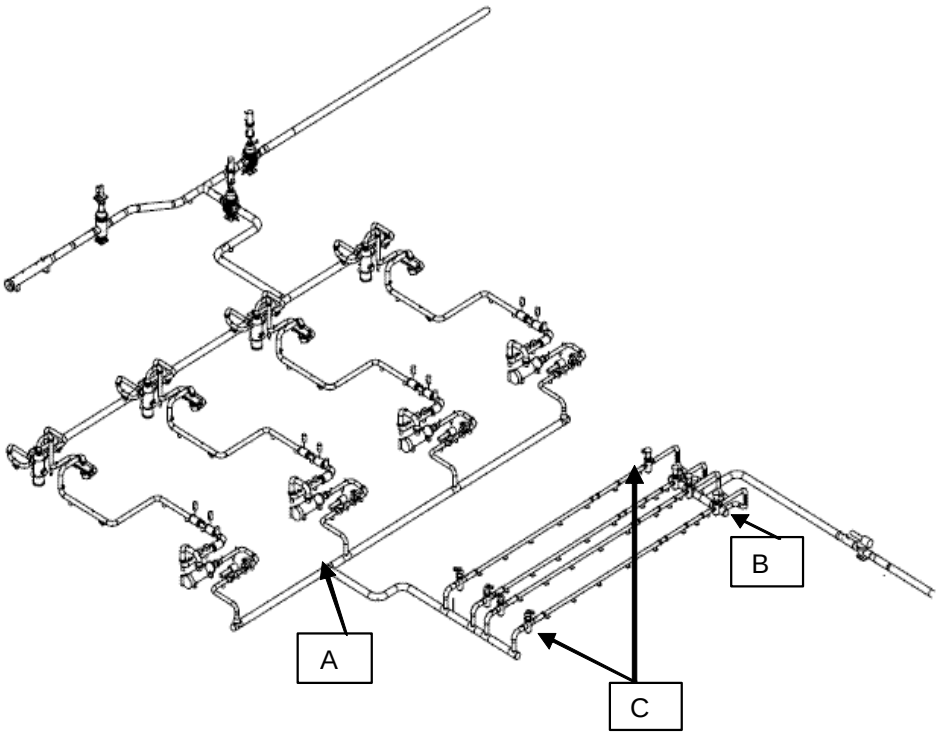

Figure 1 Geometry of the Easington measurement station. The CFD simulation geometry starts at the header inlet at the position marked A, and ends in the downstream manifold marked B.

The actual gas pressure, temperature and density in the measurement station are typical values from a given day, and can be considered to be representative for the conditions at the metering station. The gas viscosity is set to a typical value for dry natural gas. The gas flow velocities at the header are chosen to cover the variations to be expected in reality. The values are given in Table 1 .

Table 1 Flow parameters

Parameter	Value	Unit
Gas temperature	5.5	^oC
Gas pressure	64	*bara*
Gas density	60.6	kg/m^3
Gas viscosity	$1.5x10^{-5}$	$kg/m \cdot s$
Gas velocities (header)	5-10-15-20	*m/s*

Several configurations of the metering station have been used. Measurements have been carried out with 4, 3 and 2 active pipes. With 3 active pipes simulations with pipe 1, 2 and 3 respectively 1, 3 and 4 have been run. Here, pipe 1 refers to the first pipe to branch off the header etc.

An overview over the flow velocities and the Reynolds number for the different configurations is shown in Table 2. It is here assumed that the flow is evenly distributed between the individual pipes. It will be shown later that both measurement and simulations predict that the flow rate differs consistently up to 25-30 % between the individual pipes. For 4 and 3 active pipes the highest velocity is found in the header, with 2 active pipes the metering section velocity is highest. For all configurations the highest Reynolds number is in the header. The Reynolds number in the metering section is in the range $9 \cdot 10^6$ to $8 \cdot 10^7$.

Table 2 Average velocities and Reynolds number for different measurement configurations and flow rates. It is assumed that the flow is evenly distributed over the pipes.

	Velocity (m/s)				Reynolds number (-)			
Header	5	10	15	20	$2x10^7$	$4x10^7$	$6x10^7$	$8x10^7$
Pipe – 4 runs	3.9	7.8	11.6	15.5	$9x10^6$	$1.7x10^7$	$2.5x10^7$	$3.5x10^7$
Pipe – 3 runs	5.2	10.4	15.5	20.7	$1.2x10^7$	$2.3x10^7$	$3.5x10^7$	$4.7x10^7$
Pipe – 2 runs	7.8	15.5	23.3	31.0	$1.7x10^7$	$3.5x10^7$	$5.2x10^7$	$7x10^7$

3 SIMULATION MODEL

3.1 CFD Simulation Model

The CFD code *MUSIC* is used in the simulations. *MUSIC* is an in-house finite volume code developed by CMR, and has been used in simulations of pipe flow [2], [3], [4], [5].

In the simulations the gas is considered to be incompressible. The flow pressure variations are small relative to the pressure level of 64 bara, and the corresponding changes in gas density are also small.

In the simulations, equations for momentum (Navier-Stokes) and pressure are solved together with the equations for the industry standard $k-\omega$ turbulence model. Due to the high Reynolds numbers, the turbulent boundary layers at the pipe walls are thin. The wall friction is therefore modelled with wall functions. The wall is assumed to be smooth.

The numerical grid is made up by hexahedron (brick) control volumes. Up to 1.2 million volumes have been used in the simulations.

In the bulk of the simulations, the complete metering station including the pipe manifold has been part of the geometry. It is then not necessary to make any assumptions of the flow rate in each of the up to 4 metering sections, the flow rate in each pipe will be a result of the simulation. Differences in pipe flow rates will be a result of the total friction and pressure losses in the pipe network. In some simulations the mass flow rate at the end of each metering section has been set to measured or simulated values. The manifold can then be excluded from the simulation geometry. This makes it possible to use a higher grid resolution to increase the accuracy of the results.

To simplify the calculations when the total geometry including the pipe manifold is used, the outlet from the manifold is modelled as a mass sink in the manifold centre. This is considered to have little, if any, influence on the flow rate distributions in the meter runs. Also the influence on the flow profiles at the meter positions is negligible, since there are several pipe diameter distance from the flow meters down to the manifold centre.

At the inlet of the header (point A in Fig. 1) a developed axial flow profile taken from a simulation in a pipe with the header diameter and the relevant average velocity is used. In addition to the results shown here, also the case with a swirl flow at the header inlet is analyzed.

For the simulations with 3 or 2 metering section pipes in operation, the part of the closed pipe from the T-bend up to the closed valve is removed in the simulations, and the T-bend replaced with a pipe section. The same practice is also used in the downstream manifold. This simplifies and reduces the CPU-time in the simulations. The influence of this simplification on the flow rate distribution and the velocity profiles through the flow meters in the active pipes is also small.

3.2 USM Simulation Model

The flow profiles calculated by the *MUSIC* CFD code are afterwards used as input to a program for calculation of the flow profile effect for the ultrasonic flow meters in question. This analysis is based on the *USMSIM* program in the GARUSO package [6], see also [7] and [8] for related works. In this program, the average flow velocities (including the effects of the transversal flow velocity components) are calculated for each of the 6 acoustic paths of the FMC MPU 1200 ultrasonic flow meters in question. Thereafter, the integration algorithm in the MPU 1200 is applied to calculate the “measured” average axial flow velocity over the pipe cross section in the flow meters, based on the calculated average flow velocities over each of the 6 acoustic paths.

In the *USMSIM* program for simulation of the ultrasonic flow meter, cubic spline approximations are set up for the CFD-calculated flow velocity profiles in the meter cross section. The interpolation along the sound paths can then be carried out to a high accuracy. The reference average axial velocity is calculated from an accurate numerical double integral.

Details on the MPU 1200 integration algorithm specifying the positions and angles of the sound paths are supplied to Gassco from the FMC. The actual integration weights of the MPU 1200 are used with permission from FMC. These values are given as inputs to the USMSIM program.

4 FLOW SIMULATION RESULTS

The metering station is typically operated with 3 of the 4 metering sections in use. In periods the metering station is also operated with 2 or 4 metering sections in use.

Flow simulations from the header inlet and through the metering station are carried out for the following situations

- All 4 metering section pipes (pipes 1, 2, 3 and 4) are in use
- Pipes 1, 2 and 3 are in use, pipe 4 is closed
- Pipes 1, 3 and 4 are in use, pipe 2 is closed
- Pipes 3 and 4 are in use, pipe 1 and 2 are closed

Here pipe 1 refers to the first pipe to branch off the header etc.

4.1 All 4 Metering Sections In Use

The metering station is simulated with average inlet velocities of 5, 10, 15 and 20 m/s. The resulting surface relative pressure distribution[1], which also displays the pipe geometry, is shown in the upper part of Figure 2 for an average inlet velocity of 10 m/s. The maximum deviation from the 64 bara initial pressure is 0.14 bar, or 0.2 %. This shows that the incompressibility approximation is reasonable, as the corresponding variations in density would have the same deviation from the constant value. Even for an average inlet velocity of 20 m/s the maximum deviation is less than 1 %.

The flow velocities in the junctions between the header and the measurement runs are shown in the lower part of Figure 2. The flow velocity in the header will diminish after each pipe

[1] Relative to the 64 bara pressure level.

diversion as the flow rate in the header is reduced. It is also seen that the T-bends in combination with the following 90° bends acts as swirl generators, as expected.

The transverse, rotating flow is shown in the left part of Figure 3 at three different axial positions (8, 30 and 55 diameters downstream the last bend) in pipe 1 with an average inlet velocity of 10 m/s in the header. It should here be noted that the ultrasonic flow meters are installed about 55 diameters downstream the last bend. As expected, the transversal flow velocity components correspond to a swirl, and decrease downstream from the bend. However, the maximum transversal flow velocity is still 7 % of the average axial velocity at the ultrasonic flow meter installation position 55 diameters downstream the last bend. The swirl is asymmetric close to the bend. It becomes more symmetric at the meter installation position.

The axial flow velocity at the same three axial positions (8, 30 and 55 diameters downstream the last bend) in pipe 1 is shown in the right part of Figure 3. The average inlet velocity in the header is 10 m/s as for the transversal flow velocity profiles discussed above. The axial flow velocity profile is seen to be asymmetric. It is seen to be rotating downstream the pipe, when comparing the flow profile at the three axial positions. This is due to the swirly transversal flow component that also will rotate the axial flow profile. As for the transversal flow velocity profile, the asymmetry of the axial flow velocity profile decreases as the distance from the bend increases.

Due to the asymmetric configuration of the metering header, the flow distribution between the 4 metering section is not expected to be uniform. This is shown in Figure 4. There the CFD calculated average flow velocities in each metering section are shown on a relative scale for the 4 inlet header flow velocities in question (5, 10, 15 and 20 m/s). The flow rate (velocity) is lowest in pipe 1, which is the first branch to the header. The flow rate is larger in pipe 2, even larger in pipe 3, and then lower in pipe 4. The CFD simulations indicate that the relative flow distribution over the pipes is independent of flow rate. The variation in flow rate is due to a combination of local flow conditions in the T-bend junction together with the line friction and pressure losses due to pipe bends and entrance losses to the manifold. In addition to the results from the CFD simulations, measurements from the metering station when all four metering sections are in use are shown. In this case, the inlet header velocity is 5.7 m/s. It is seen that qualitatively, the measurements show the same distribution in flow velocity over the four metering section as found from the CFD simulations. Quantitatively, the largest difference is seen for pipe 1.

4.2 2 or 3 Metering Sections In Use

In order to cover normal operation configurations of the metering station, also simulations with 2 or 3 metering sections in use have been carried out. For 3 metering sections in use two configurations have been simulated. These are:

- Pipes 1, 2 and 3 are in use, pipe 4 is closed
- Pipes 1, 3 and 4 are in use, pipe 2 is closed

In addition the following configuration with 2 metering sections has been simulated:

- Pipes 3 and 4 are in use, pipe 1 and 2 are closed

As for the case with all 4 metering sections in use, CFD simulations have been carried out for average inlet velocities at the header of 5, 10, 15 and 20 m/s.

For simplicity, only results for the relative flow distribution between the pipes are presented here. In Figure 5 the results for the two configurations with 3 metering sections in use are shown. As for the case with all 4 metering sections in use, there is an asymmetry in the velocity distribution between the metering sections. It is also seen that the correspondence between simulations and measurements is good.

In Figure 6, the similar results are shown for 2 metering sections in use. In this case, no comparisons with experimental results have been carried out.

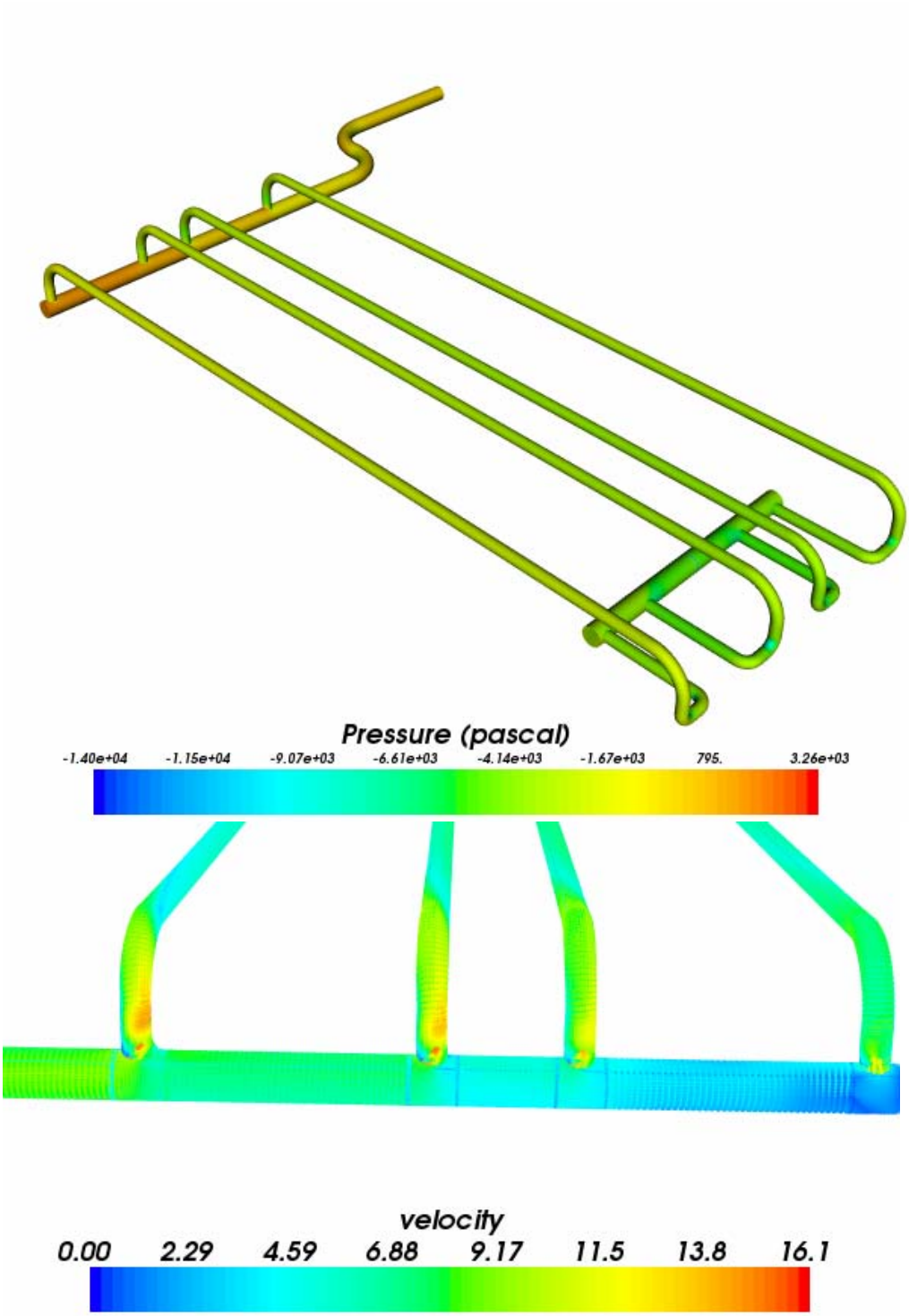

Figure 2 *Upper figure: Plot of pipe surface relative pressure. The difference between maximum and minimum pressure in the geometry is 0.17 bar, and the differential pressure between inlet and manifold 0.08 bar. Lower figure: Velocity vector magnitude. It can be seen that the T-bends in combination with the 90° bends generates rotation. In both cases the average inlet velocity of the header is 10 m/s.*

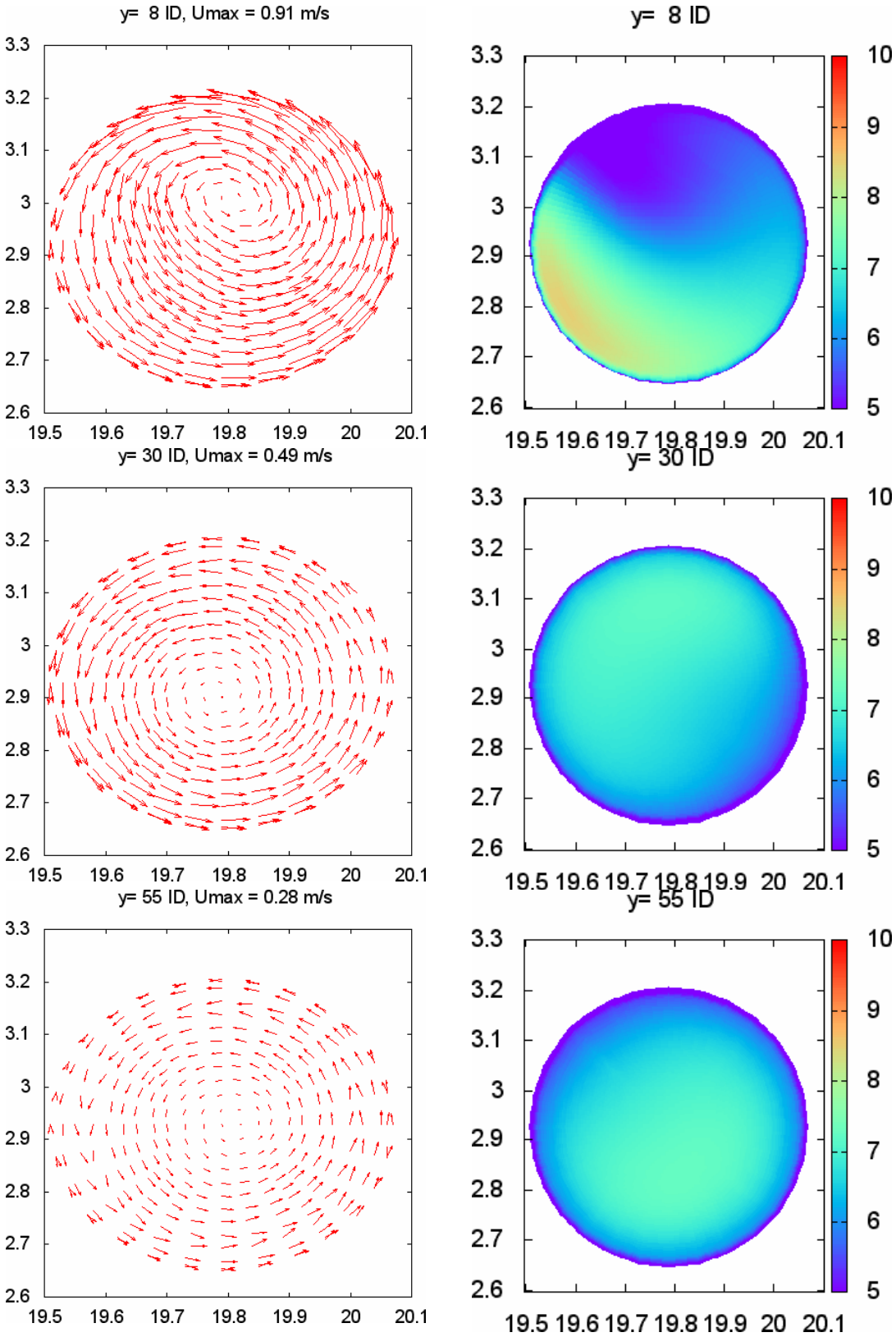

Figure 3 *CFD simulated transversal (left) and axial (right) flow velocity profiles in pipe 1 in a cross-sectional cut plane at 8, 30 and 55 diameters downstream the bend. The header velocity is 10 m/s. The view direction is downstream towards the meter. The ultrasonic flow meter is located about 55 diameters downstream the bend.*

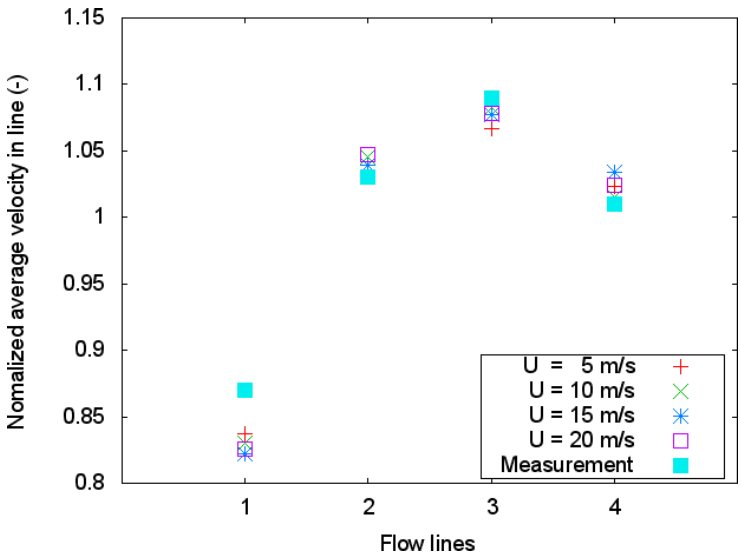

Figure 4 *CFD simulated and measured relative flow distribution over the different metering sections when all metering sections are in use. Flow line 1 is the first branch to the header, the other are numbered in increasing order.*

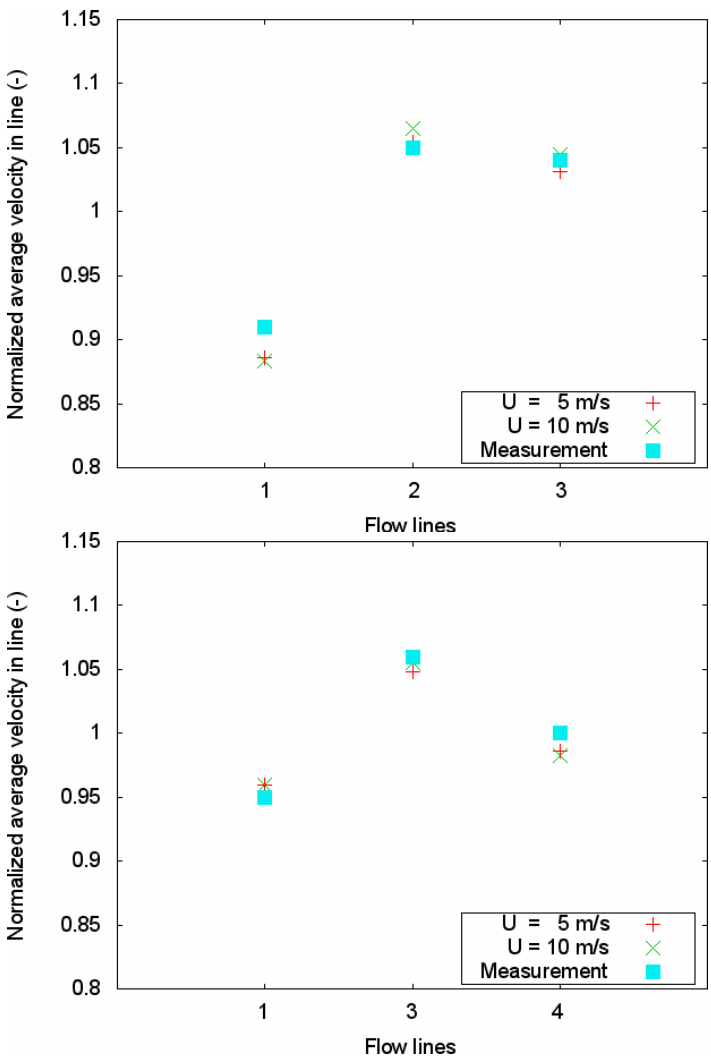

Figure 5 *CFD simulated and measured relative flow distribution over the different metering sections when 3 metering sections are in use. Flow line 1 is the first branch to the header, the other are numbered in increasing order.*

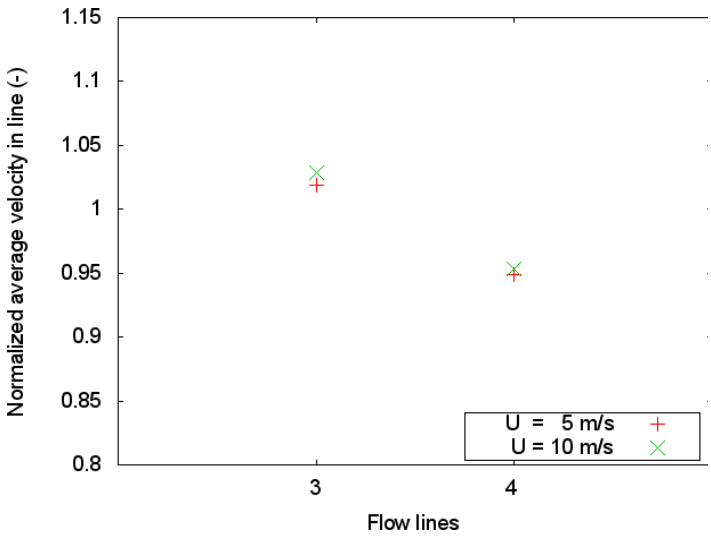

Figure 6 CFD simulated relative flow distribution over the different metering sections when 2 metering sections are in use. Flow line 1 is the first branch to the header, the other are numbered in increasing order.

5 MPU 1200 INTEGRATION ANALYSIS

As mentioned above, the average flow velocities (including the effects of the transversal flow velocity components) are calculated for each of the 6 acoustic paths of the FMC MPU 1200 ultrasonic flow meters in question. Thereafter, the integration algorithm in the MPU 1200 is applied to calculate the "measured" average axial flow velocity over the pipe cross section in the flow meters, based on the calculated average flow velocities over each of the 6 acoustic paths.

5.1 Flow Calibration

The ultrasonic flow meters are flow calibrated at Advantica before installation at Easington. Hence, the present analysis covers the deviations from the flow calibration conditions.

The flow calibration conditions are considered here as a well developed symmetric flow profile. This is modelled by the same CFD model for a long, straight pipe with the flow parameters and grid resolution as used elsewhere in this report. For this flow profile, the simulation of the MPU 1200 integration gives an over-prediction of average axial flow velocity from 0.15 – 0.17 % for Reynolds numbers in the relevant range from 10^7 to 10^8. This corresponds well with other work [5].

In the following part of this report, 0.15 % is therefore subtracted from the deviation from reference percentages, in order to study the deviation from flow calibration to installation at LFR Easington.

5.2 All 4 Metering Sections In Use

The ultrasonic flow meters have been installed with a straight upstream pipe length to the closest upstream bend of 54.1 diameters. The length of the spool piece is 2.4 diameters.

In the analysis, simulations have been carried out with (imagined) flow meter installations with from about 10 diameters to more than 55 diameters of straight upstream pipe, in order to study the effect of the long straight upstream pipe section. The results for this analysis are presented in Figure 7, where the deviation from reference are shown for all 4 metering sections for an inlet average flow velocity at the header of 5, 10, 15 and 20 m/s. It can be

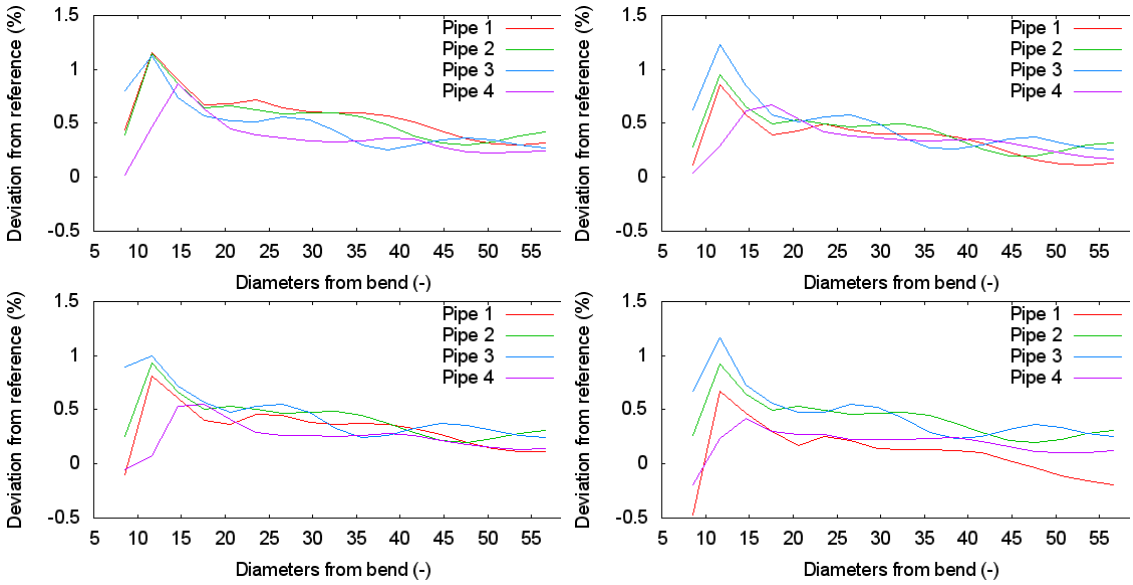

Figure 7 *Installation effect on the ultrasonic flow meters relative to the reference velocity, for imagined installations of the ultrasonic flow meters. All 4 metering sections are in use. The results are shown with an average inlet flow velocity in the header of 5 m/s (upper left), 10 m/s (upper right), 15 m/s (lower left) and 20 m/s (lower right)*

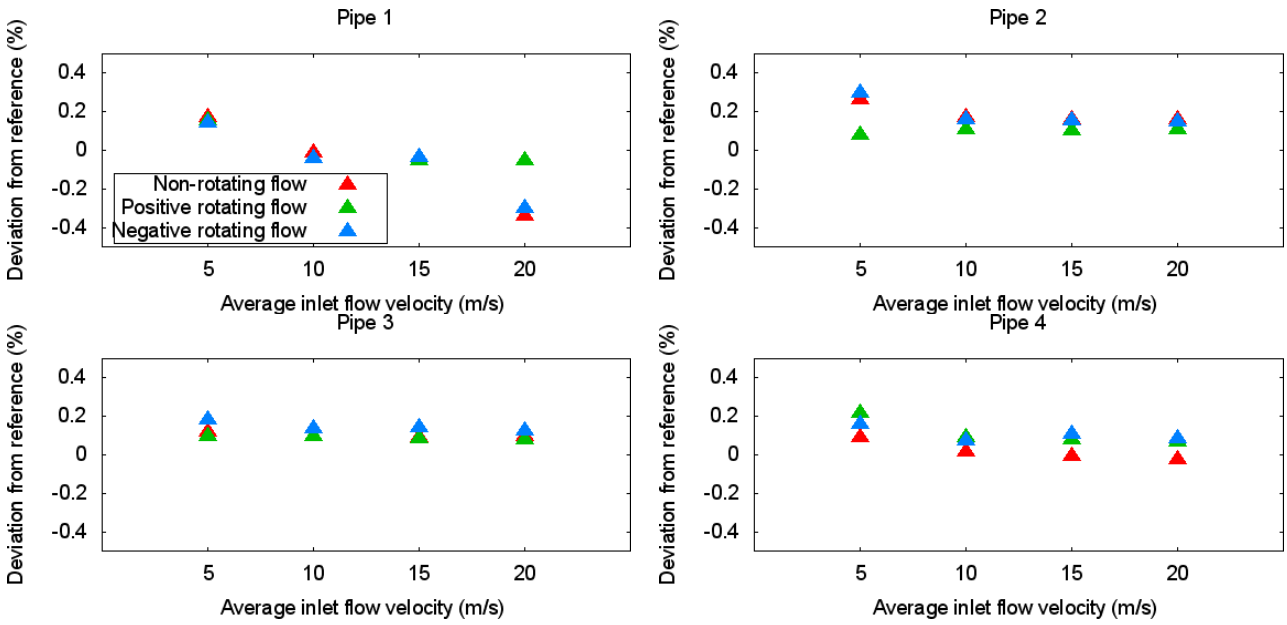

Figure 8 *Installation effect on the ultrasonic flow meters relative to the flow calibration, for the actual installation of the ultrasonic flow meters. All 4 metering sections are in use.*

seen that qualitatively, the results are quite similar over the flow velocity range. Furthermore, it is seen that if the flow meter were installed with a straight upstream pipe section of about 20 diameters or less, deviations from the flow calibration of up to 1 % could be expected due to large asymmetries in the flow profiles. At the relevant installation point of the ultrasonic flow meters, the deviation from reference is typically much less.

This is illustrated better in Figure 8, where the deviation from the flow calibration is shown as a function of average inlet flow velocity at the header. It is seen that the installation effect typically is in the order of about 0.2 % or less. All points except one are less than 0.3 %, and all points are less than 0.4 %. In the same figure, also results with swirly inlet flow profiles to the header are shown. It is seen that this does not affect the results significantly. This is expected as the T-bends branching off from the header have strong impact on the flow profiles.

5.3 2 or 3 Metering Sections In Use

Deviation from the flow calibration as a function of average inlet flow velocity at the header is shown for the two configurations with 3 metering sections in use in Figure 9 and for the configuration with 2 metering sections in use in Figure 10. The results are comparable with the results with all 4 metering sections in use.

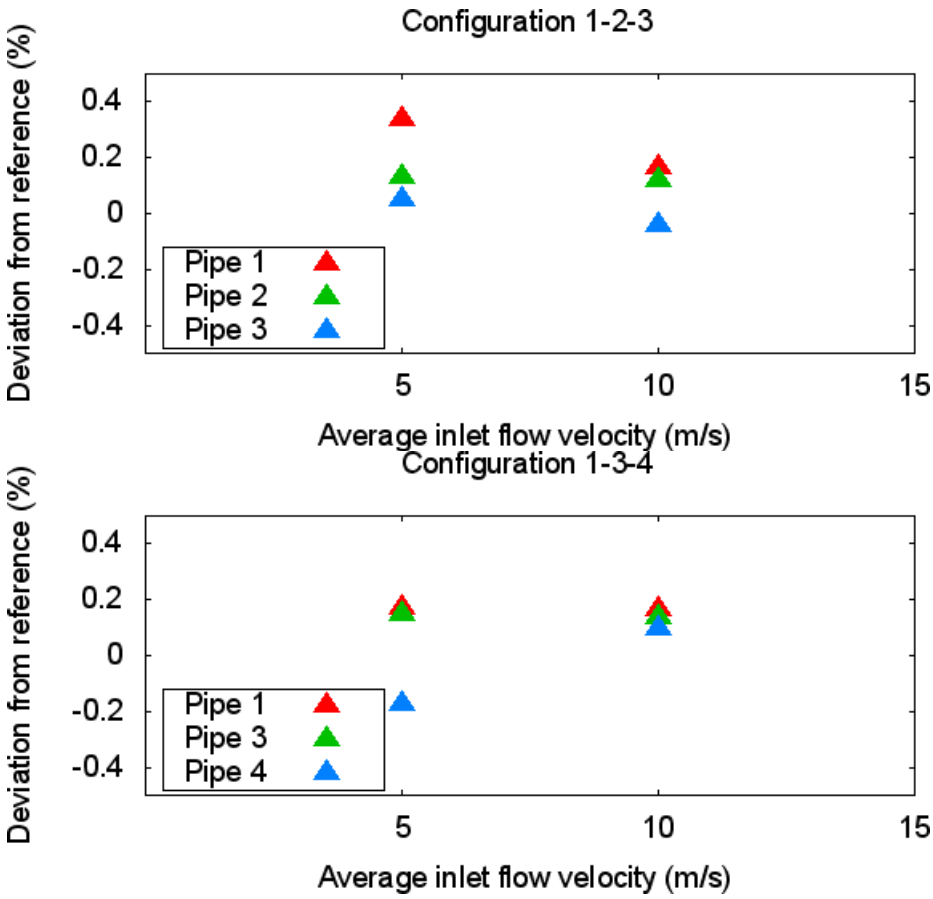

Figure 9 Installation effect on the ultrasonic flow meters relative to the flow calibration, for the actual installation of the ultrasonic flow meters. 3 metering sections are in use.

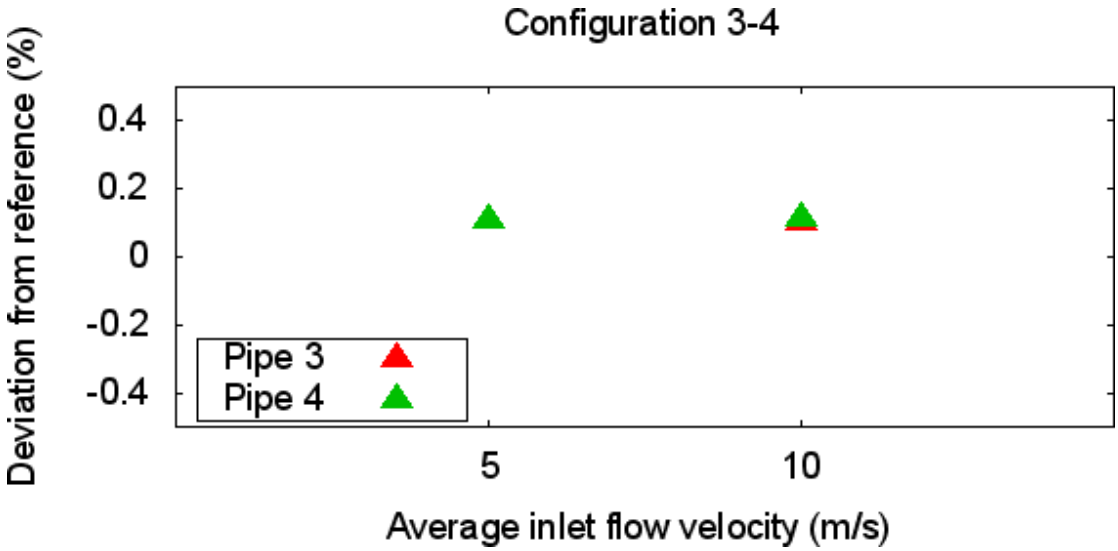

Figure 10 Installation effect on the ultrasonic flow meters relative to the flow calibration, for the actual installation of the ultrasonic flow meters. 2 metering sections are in use.

6 DISCUSSION AND CONCLUSIONS

The metering station at the Langeled Receiving Facilities in Easington consists of 4 parallel metering sections each equipped with ultrasonic flow meters. After start-up of the metering station it has been observed that the measured flow velocity profiles have been asymmetric. This has raised the question about a possible influence of the installation effect (through asymmetric flow profiles) on the measured flow rates. Based on this, the flow profiles in the metering station have been studied by CFD modelling and thereafter simulation of the ultrasonic flow meter.

The CFD analysis indicates that the flow velocity is not uniformly distributed over the 4 metering sections. This is found for all flow rates and all pipe measurement configurations (2, 3 or 4 metering sections active). In all configurations pipe 1 (the first pipe to branch off the header) has the lowest flow. Largest flow is found in pipe 3 for the 1-2-3-4 and 1-3-4 measurement configurations, and in pipe 2 in the 1-2-3 measurement configuration. With the same header flow inlet conditions the simulations predict that the relative distributions are almost independent of flow rates in the range used in the investigation.

For the configuration with all 4 metering sections in operation, the simulations have been compared with measurements for one flow rate. Generally, the simulated and measured data agree well. Largest offset is seen for metering section 1, where the simulations show a smaller relative value than the measurements, 0.83 against 0.87 for the simulations. For the other pipes the differences are smaller. Comparisons with measurements have also been carried out for the two simulated configurations with 3 active metering sections. Also here, the simulated and measured data agree well.

The simulations indicate further that the axial flow velocity profile through each of the 4 metering sections is asymmetric. It is also rotating as the gas flows downstream through the metering sections. In addition, there is a asymmetric swirly transversal flow velocity profile. This is in agreement with estimates given in literature [9], where developed flow is reached first after 64-84 ID for the Reynolds numbers used here. A swirly transversal flow is also expected because the double bend out of plane (including one T-bend) upstream each of the metering sections is traditionally found to be a strong swirl generator.

When the flow velocity profiles in the metering sections are established by CFD simulations, the effect of the asymmetric axial and transversal flow velocity profiles on the ultrasonic flow meters is analyzed by a dedicated computer program. In addition to simulation of the effect on the ultrasonic flow meters in the position where they are installed in practice, also other virtual installation locations have been analyzed. The main trend is that the deviations between the ultrasonic flow meter output and the reference are large and variable (up to about 1 %) with potential installations at the start of the straight measurement sections. With virtual installations 20-30 diameters after the bend, the deviation is smoother and decaying downstream in the pipe towards the actual meter installation. The bulk of the deviation curves are oscillatory after 20-30 diameters. This reflects the flow rotation in the pipes; the axial flow has a skew distribution in the upstream pipe section. The position of the maximum velocity in the pipe cross-section will also rotate downstream in the pipe. The flow rotation is not in phase between the different pipes. This is reflected in the oscillations in the deviation curves, which are not in phase between the pipes.

The results from the simulation of the ultrasonic flow meters have been corrected for flow calibration. The flow calibration effect has been simulated by assuming a well developed symmetric flow profile. When the correction for flow calibration has been carried out, the effect of the asymmetric flow profiles is found for all cases except one, the deviation from reference at the meter installations is less than ± 0.3 %.

7 REFERENCES

[1] http://www.fmctechnologies.com/MeasurementSolutions/ProductsServices/Products/GasMeasurement/MPU1200.aspx

[2] Frøysa, K.-E., Hallanger, A. and Lunde, P.: "K – factor of the Fluenta FGM 100 Flare Gas Meter for the 'Laminaria and Corallina Development Project'", CMR Report CMR-98-F10012, Christian Michelsen Research AS, Bergen, Norway (1998) (Confidential).

[3] Frøysa, K.-E., Hallanger, A. and Lunde, P.: "K – factor of the Fluenta FGM 100 Flare Gas Meter for the 'Valhall/Hod Modification Project'", CMR Report CMR-98-F10023, Christian Michelsen Research AS, Bergen, Norway (1998) (Confidential).

[4] Hallanger, A. .: "Evaluation of oil metering station on Oseberg Sør'", CMR Report CMR-01- F1024, Christian Michelsen Research AS, Bergen, Norway (2001) (Confidential).

[5] Hallanger, A., Frøysa, K.-E. and Lunde, P.: "CFD simulation and installation effects for ultrasonic flow meters in pipes with bends", Int. J. of Applied Mechanics and Enginering, Vol 7, Number 1, 33-64 (2002)).

[6] Lunde, P., Frøysa, K.-E. and Vestrheim, M.: "GARUSO – Version 1.0. Uncertainty model for multipath ultrasonic transit time gas flow meters ", CMR Report CMR-97-A10014, Christian Michelsen Research AS, Bergen, Norway (1997).

[7] Lunde, P., Frøysa, K.-E. and Vestrheim, M.: "GERG project on ultrasonic gas flow meters, Phase II", GERG technical monograph TM11, Groupe Européen de Recherches Gaziéres, The Netherlands, VDI Verlag, Düsseldorf, (2000).

[8] Lunde, P. and Frøysa, K.-E.: “Handbook of uncertainty calculations. Ultrasonic fiscal gas metering stations,” Issued by Norwegian Society of Oil and Gas Measurement, Norwegian Petroleum Directorate and Christian Michelsen Research AS, Norway (free download available from www.nfogm.no) (2001).

[9] Schlichting, H.:”Boundary layer theory”, 7th edition, McGraw-Hill, New York, 1979.